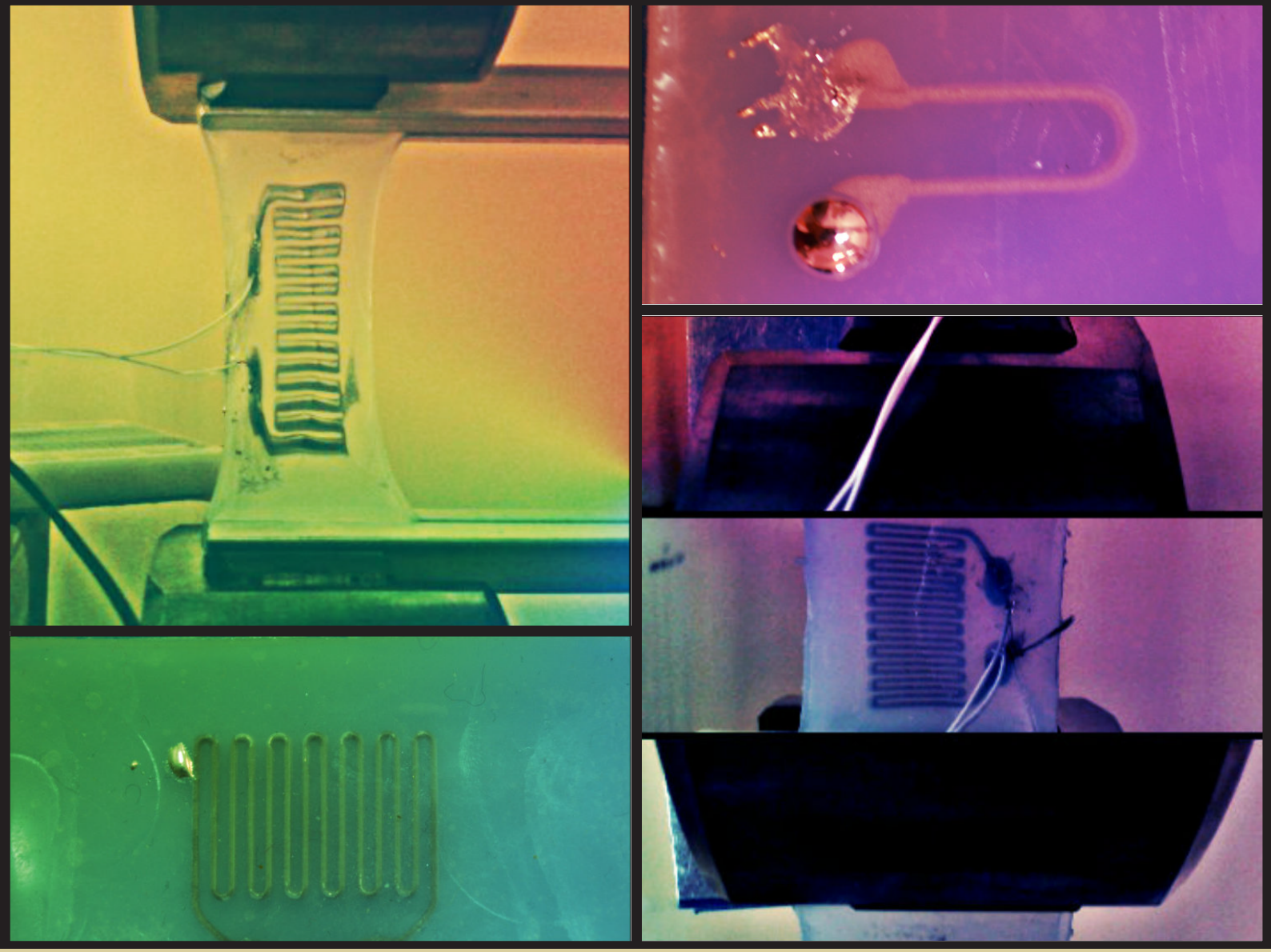

Ana Filipa Soares Tomé

Soft Sensors for Soft and Wearable Robots

Dissertação de Mestrado Integrado em Engenharia Biomédica apresentada no Departamento de Física da Faculdade de Ciências e Tecnoogia da Universidade de Coimbra

Setembro 2014

· U C ·

Universidade de Coimbra

• U C •

FCTUC FACULDADE DE CIÊNCIAS
E TECNOLOGIA
UNIVERSIDADE DE COIMBRA

Ana Filipa Soares Tomé

Soft Sensors for Soft and Wearable Robots

Dissertation presented to the University of Coimbra in order to complete the necessary requirements to obtain the Master's degree in Biomedical Engineering.

Supervisors:

Dr. Mahmoud Tavakoli

Prof. Lino Marques

Coimbra, 2014

This work was supported by:

INSTITUTE OF SYSTEMS AND ROBOTICS
UNIVERSITY OF COIMBRA

Agradecimentos

O final do meu percurso académico é uma ocasião em que inevitavelmente surgem em retrospectiva os momentos e as pessoas que contribuiram para o seu sucesso e o tornaram tão especial.

Em primeiro lugar devo um enorme agradecimento a todos os que me acompanharam e ajudaram, durante este ano no ISR, sempre que isso esteve ao seu alcance. Ao Doutor Mahmoud Tavakoli e ao Professor Lino Marques pelo tempo dedicado ao acompanhamento do meu projecto e pela orientação e exigência para que este se concretizasse em algo de que hoje me orgulho bastante. Aos meus colegas do LSE, em especial, Tifi, Daniel e Ricardo, pelos conhecimentos transmitidos e pelas lições valiosas à hora de almoço que tornaram tudo mais simples em cada dia. Não esqueço o Baptiste e a Ritinha, que durante meses estiveram ao meu lado, dando sempre o seu parecer sincero, motivando-me e fazendo-me acreditar que o sucesso é sempre possível. Concluir este projecto não teria sido possível se não existissem como exemplo estes dois "companheiros de guerra" ao longo deste ano.

Em Coimbra conheci pessoas extraordinárias e aprendi lições valiosas, que fazem justiça àqueles que dizem que nem sempre nos livros está tudo o que precisamos de saber. Ao meu lado, a revirar livros, sebentas e a riscar quadros com esquemas e equações intermináveis estiveram a Ritinha, o Baptiste, a Varalonga, a Mariana Santos, a Natasha, o Devesa, o Pina e a Margarida Martins. Ensinaram-me o significado de trabalho de equipa, paciência, garra, esforço e acima de tudo ensinaram-me a conciliar as responsabilidades com os momentos para descontrair e ser feliz.

Incluo mesmo todos os que tive o prazer de conhecer durante estes cinco anos quando expresso o meu agradecimento por me terem sempre feito sentir em casa. As coisas têm outro gosto quando se criam laços como estes pelo caminho. Obrigada Rita, Margarida, Inês, Kiki, Márcia, Chanel e Gradil, por me ajudarem a descontrair, melhorar, rir e crescer. Que passem os anos e que consigamos sempre que o longe se faça perto.

O meu último e mais importante agradecimento é dirigido aos meus pais, as duas pessoas que me viram crescer e que me transmitiram os seus valores, a sua capacidade de trabalho e a força para nunca desistir. Agradeço-vos toda a paciência para me acompanhar em inscrições, mudanças, festas e momentos de maior tensão. São o meu maior e melhor exemplo e assim o meu trabalho é também vosso, pela forma como me ensinaram a encarar os desafios.

Abstract

With a growing need for safer human-robot interactions and taking the human skin properties as biological inspiration, the technological field of soft sensors has grown considerably in the last few years. Conventional tactile sensors integrated on robot gripers are nowadays available in multiple formats. Nonetheless, most of the tasks performed by robots demand complex rotational movements. Sensors adaptable to their host can turn robotic devices into safer technology to interact with and are easier to integrate in wearable devices since they do not interfere with their mechanical performance. The ease of access to soft materials and fabrication methods of customized objects through 3D printing, allows the development of soft sensors with desired geometries using low cost and simple methods.

This work addresses the development of two distinct soft sensors, with embedded liquid-metal microchannels, by casting a liquid elastomer into 3D printed molds engraved with micro-dimensioned features. The first type of stretchable sensor, was designed for strain-sensing and can be applied in multiple devices to give information about joint angles and posture of prosthetic hands. The second designed sensor is intended to detect contact forces during manipulation and assembly.

This project is a good example of how a mix of multidisciplinary knowledge coming from materials engineering, electronics, and robotics can form the basis of engineering state-of-art devices which can contribute to the further study and development of artificial skins with multiple sensing capabilities.

Keywords: Soft Robots; Wearable Robots; Soft and Elastic Sensors; Tactile Sensors; Stretchable Sensors; EGaIn; MEMS;

Resumo

Devido a uma crescente necessidade de segurança durante a interação entre *robots* e humanos, tomando a pele humana como inspiração biológica, o campo tecnológico de sensores flexíveis tem crescido consideravelmente nos últimos anos. Sensores tácteis convencionais integrados em garras robóticas estão actualmente disponíveis comercialmente em múltiplos formatos. No entanto, a maioria das tarefas desempenhadas por *robots* exigem movimentos rotacionais complexos. Sensores adaptáveis ao seu hospedeiro podem tornar aparelhos robóticos em tecnologias mais seguras e acessíveis uma vez que são capazes de se adaptar sem interferir com o seu desempenho mecânico. A facilidade de acesso a materiais flexíveis e métodos de fabrico de objetos personalizados através de impressão 3D, facilita o desenvolvimento deste tipo de dispositivos, com geometrias desejadas, usando métodos simples e de baixo custo. Este trabalho aborda o desenvolvimento de dois tipos distintos de sensores complacentes com microcanais de metal líquido incorporados através da deposição de um elastómero em moldes impressos em 3D com detalhes na ordem dos micrómetros gravados na sua superfície. O primeiro tipo de sensor extensível, foi desenhado para medir deformação e pode ser aplicado em múltiplos aparelhos para obtenção de informação acerca do ângulo de juntas e postura de mãos robóticas prostéticas. O segundo sensor desenhado destina-se à detecção de forças de contacto durante actividades de manipulação e montagem.

Este projecto é um bom exemplo de como conhecimento multidiscplinar desde engenharia de materias, electrónica e robótica permite formar a base de um aparelho funcional que pode contribuir para o estudo e desenvolvimento futuros de uma pele artificial com múltiplas capacidades sensitivas.

Palavras-Chave: Robôs Complacentes; *Wearable* Robots; Sesnores Complacentes e Elásticos; Sensores de Tacto; Sensores Extensíveis ;EGaIn; MEMS;

Contents

Acronyms

3D Three-Dimensional

ABS Acrylonitrile Butadiene Styrene

EGaIn Eutectic Gallium-Indium

FDM Fusing Deposition Modeling

MEMS Microelectromechanical Systems

PDMS Polydimethylsiloxane

PLA Polyamide

PVDF Distal Interhalangeal joint

SLA Stereolithography

SLS Selective Laser Sintering

List of Figures

List of Tables

Chapter 1

Introduction

For both humans and robots sensing is a very important tool to interact with the environment. For humans, sensing provides recognition of objects and their properties, making it easy to correctly grab and manipulate them. For robots, especially the ones that require human interaction, sensing improves their performance and more importantly, it reinforces the manipulation security, since it gives information about the objects that are being handled and helps robots to adapt their behaviour. The concept of a robot as an exclusive industrial tool is fading, and humanoids, assisting, medical and bio-robots are making their way into daily routines of specialists in several areas. This implies human-robot interaction, which needs to be safe and have natural behaviour and appearance. These requirements have increased the interest for integration of soft materials in novel robotic systems and motivated the development of wearable and prosthetic devices, such as the Yale open hand project [1], health monitoring wearable sensors [2] or wearable assistance robots [3].

Soft mechanisms are safe to interact with and are very adaptive to their environment. One of the specific areas of research in soft mechanisms is soft and wearable sensors, and soft materials are being considered for fabrication of strain and pressure sensors that can easily conform to robots and make their interaction with the environment easier.

These materials can sustain large elongations, being able to stretch several times their rest length, and enable rich range of electronic and sensing functionalities. This is very important in biomechanics and robotics so that electronic components have good conformation to joint rotations and do not interfere with the natural mechanics of the host.

Soft sensors that are highly deformable are critical for the evolution of areas such as wearable robots, haptics, humanoid robots and medical robots. Simple tasks as shaking someone's hand, or grabbing brittle objects, would not be possible without haptic information which is a natural gift in humans.

The human body is able to sense position and to provide orientation to its limbs. Numerous mechanoreceptors in the human skin can sense strain and pressure. Figure 1.1 shows the physical location of some of the mechanoreceptors.

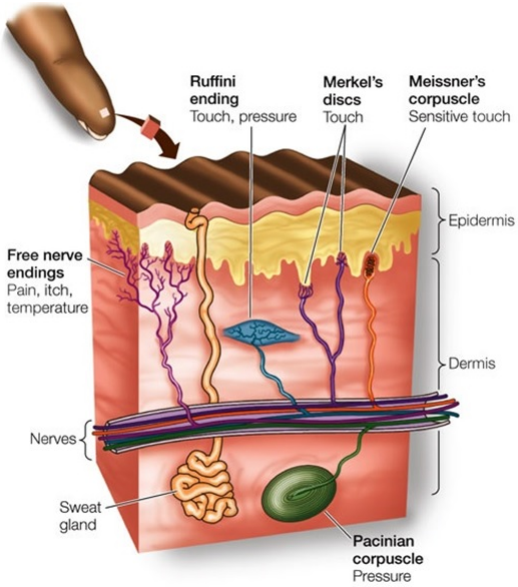

Figure 1.1: A small patch of skin with a variety of sensory cells, that can sense temperature, pressure, texture, pain, touch, and itch [4].

The human sense of touch deals with spatiotemporal perception of external stimulus through different receptors that can be found at different depths in the skin, as it is shown in Figure 1.1. They can be mechanoreceptors to detect pressure/vibration, thermoreceptors to measure temperature or nocioreceptors which can detect damage or pain. When in contact with an object the skin conforms to its surface and projects the deformation to its many receptors. In a simple way, this is what makes the identification of properties of touched and manipulated objects possible.

It is frequently necessary to detect slip or to roll an object between fingers without dropping it. As in humans, tactile sensing can help understand the behaviour that is required to correctly perform these tasks with a prosthetic hand. The way an object is "sensed" when it is touched is responsible for its manipulation.

An important use of bioinspired sensors is to provide feedback in prosthetic devices, which was first achieved in the 1970's. Pfeiffer et al. developed a prosthetic device that was intended to provide sensing feedback to patients with absence of sensation. The used sensors were flexible mercury strain gauges, and gave patients the ability to differentiate between no force and medium force [5] [6]. This was an early study that was useful to conclude that a lot of research work was left to do in this area. As efforts started to emerge to study this technology with significant depth, interesting applications were revealed. Romano et al. accomplished the implementation of tactile sensing in a commercial robotic platform. The invention used capacitive sensors, in a robotic gripper fingertip that was then able to pick up and put down objects in a selected location [7].

Alongside, other research groups focused on the implementation of tactile and strain flexible sensors on wearable assistance robots. In 2011 Park et al. described the design of a soft device to treat pathologies associated with neuromuscular disorders. Three pneumatic artificial muscles provided assistance and physical support to improve mobility and increase stability, while improving and encouraging rehabilitation.

The prototype was equipped with embedded strain and pressure sensors. The strain sensors provided information about changes in the joint angle, and the pressure sensors detected the contact of the foot with the ground [8]. The same research group also developed an elastomer sleeve, also for assistance robots, that when wrapped around a joint used its actuators and stretchable sensors to monitor and assist lower and upper body tasks [3]. Soft wearable sensing suits were presented too, either for biomechanical measurements [9] or assistance in motor tasks in patients with limited motor control [10].

Other applications included the integration of tactile sensing arrays in micromanipulators, or their encapsulation in a thin elastic base glove [11] [12]. Figure 1.2 gives a visual overview of some of the most relevant applications of soft sensors in robotics and wearable devices, in chronological order. Figures 1.2 c) d) and f) show different studies from the same research group that have improved their work through the years. Figure 1.2 a) shows an early attempt to fabricate a sensitive glove to improve dexterity of robots. The studies illustrated in figures 1.2 b) and e) also intend to improve the dexterity of robots by simply integrating tactile sensors in their grippers, which can be considered much simpler than the application mentioned before.

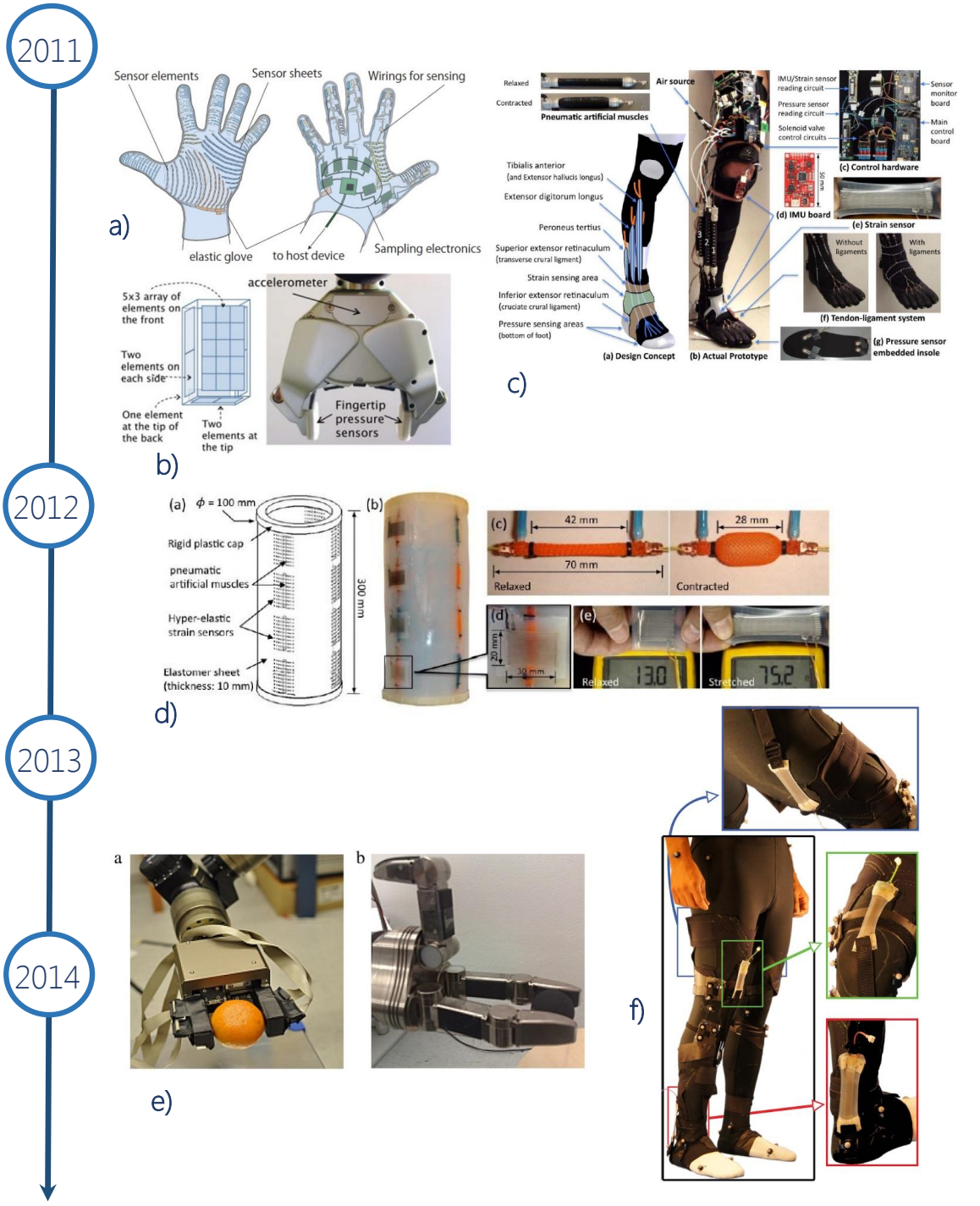

Figure 1.2: Chronological overview of applications of soft sensors on wearable robotics and biomechanical devices: a) Tactile sensing glove based on branch shaped tactile sensor sheet [11]. b) Pressure sensors attached to robotic fingertips under a silicone rubber coating [7]. c) Soft sensors on an active soft anklefoot orthotic device powered by pneumatic artificial muscles [8]. d) Integration of soft strain sensors on a soft orthotic device for assistive body motion [3]. e) Flexible tactile sensor mounted on the fingers of a robotic gripper [12]. f) Soft strain sensors on a sensing suit for lower limb measurements [9].

1.1 Motivation and Goals

The previously mentioned applications are recent and use flexible materials that are small, thin and adaptive to their host. The main inspiration for them was the human skin, which has multiple small sensors and provides high resolution tactile information to humans.

Up until recently, tactile flexible technologies were a subject of minor interest since the fabrication methods and materials were complex and expensive. 3D printing technologies have opened up new frontiers, since they have enabled the access to simpler and cheaper manufacturing methods and tools of design and fabrication. Currently, one is able to design and print simple molds that can be used to fabricate patterned flexible objects by simply pouring the desired material into them. The study, design and fabrication of small flexible sensors, are nowadays easier due to simpler methods of microfabrication.

The main goals of this project were to expertise the fabrication process, including design, fabrication and test of two different types of flexible sensors, one for strain sensing and a second one for pressure sensing. The sensors were intended to have metal-embedded channels with dimensions in the μm scale, so they could be adapted to a robotic prosthetic hand. The metal-embedded microchannels were also designed to give information based on their deformation and consequent change of electrical resistance of the liquid conductive metal inside them. Finally the integration of the fabricated sensors in the fingers of the ISR-Softhand was also studied, being that the sensors dimensions were conditioned by the dimensions of a prosthetic finger, shown in figure 1.3. This is an example of one of the fingers developed within the ISR-Softhand project, in which the fabricated sensors could be placed.

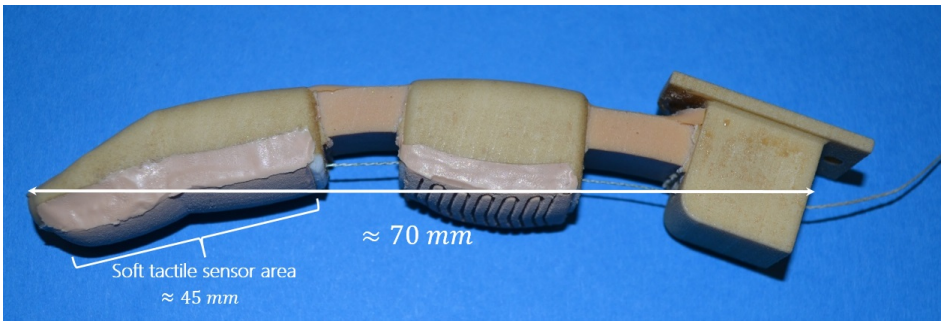

(a) Example of fabricated finger with identification of the intended soft tactile sensor area.

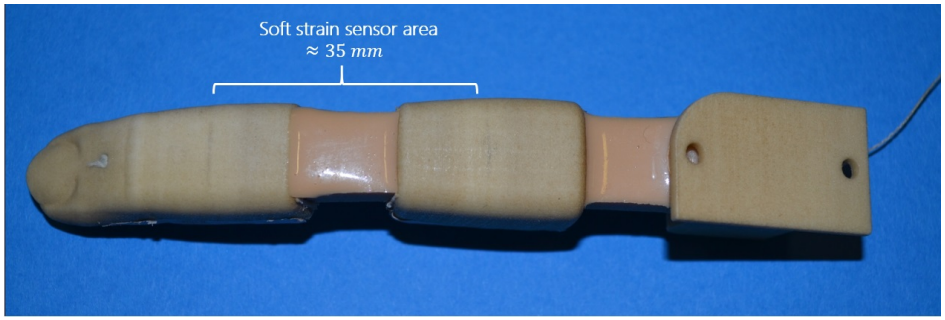

(b) Top view of fabricated finger with identification of the intended soft strain sensor area.

Figure 1.3: 3D printed fingers, with Vytaflex to mimic the compliance of human joints.

1.2 Thesis Overview

This dissertation is divided into five chapters. The first chapter presents the framework, motivation and thesis organization. The second chapter is dived in two main parts. The first sums up the technical concepts behind stretchable electronics and more specifically tactile sensors, and the second one gives an overview of the work done so far in that technological field.

The third chapter includes the design of the molds fabricated by 3D printing technology for patterning the microchannels in the chosen flexible materials and the casting, bonding and injection steps towards the fabrication of the soft sensors. Every decision towards the choice of the materials is also justified as well as the chosen methods and their expertise process. The problems faced through the fabrication of the prototypes are reported at the end of this chapter so that future work on the studied area can be done more effectively.

The fourth chapter comprises the characterization trials of the sensors. The experimental setups and used materials are described and the results from the tests are presented. A theoretical study is demonstrated and the behaviour of the devices is compared to the studied information.

In the fifth and last chapter the general conclusions are summarized and future work is discussed.

Chapter 2

Related Literature

In this chapter an overview of tactile sensing technologies is presented, even though more emphasis is given to stretchable tactile sensors. The basic theoretical concepts are explained and some of the most relevant examples for this project are mentioned. Namely this chapter will give an overview in:

- Human skin, as an inspiration for integration of soft sensing devices in robotics.
- Conventional tactile sensing technologies.
- Flexible tactile sensors and most commonly used materials to their fabrication.
- Work done so far in the field of flexible tactile sensors separated by type of transduction principle.

Since the human skin has several important properties that can serve as inspiration to design and develop tactile systems, a brief overview of the human skin and its sensing abilities is first mentioned. Since this project does not intend to completely mimic the features of the human skin, only the relevant advantages of this human tissue are resumed.

2.1 Tactile Sensing

2.1.1 The Touch Sense

The human senses such as sight, touch, taste, smell and sound enable the interaction with the surrounding environment [5]. The touch sense deals with spatiotemporal perception of external stimulus through many receptors that can be found at different depths in the skin [13].

Humans rely on this sense to touch objects and manipulate them, which is even more relevant in the absence of other sensing abilities. Simple tasks such as manipulating an egg without breaking it are intuitive for humans, even though it comprises complex neurological processes. It is also frequently necessary to detect slip or roll an object with the fingers without dropping it. In humans touch helps to understand the right behaviour to avoid dropping or breaking an object, even though it is something intuitive and most of the times not even perceptible [13]. Touching an object enables the identification of properties such as shape, size, weight and texture that are transmitted to the brain through sensory receptors. The information received by the brain is responsible for manipulation, and a constant feedback ensures that the objects do not slip or break [5]. The human skin is a version of a compliant sensor with several important properties [14].

- It has the ability to conform to the surfaces of objects when in contact with them, projecting the deformation to its many receptors [14].
- It is a robust tissue [14].
- It is stretchable, being able to stretch many times its rest length [14].
- It has a lifespan as long as a human's life [14].

The skin of a human fingertip has more than 2500 touch receptors. They can sense pressures of approximately $100Pa$ (Pascal) and remain functional even at over $1000KPa$ [14]. When robots are expected to accomplish tasks that require careful manipulation of objects, sensory abilities as the ones possessed by humans are important to provide the feedback to correctly interact with them. Re-engineering some of the skin sensing properties into a reasonable working sensor is an open scientific problem that is currently being investigated in many research centres. This section is divided in two different parts so that the conventional tactile sensors and technologies can be clearly separated from stretchable electronics and sensors. The goal is to show the evolution from rigid technologies towards stretchable ones, being the second the main focus of this project.

2.1.2 Conventional Tactile Sensing Technologies

Tactile sensing was first considered a subject of interest in the 1970's, even though it has been for several years a minor research area within major projects. Even though, it was established that the use of tactile sensors improved the quality of robots, turning them safer to manipulate specially in human-robots interactions, tactile sensing became more appealing in situations in which other sensing technologies, such as sight, failed to be a good sensing modality [5]. The most common tactile transduction techniques use capacitive, piezoresistive, piezoelectric and resistive methods.

Here a short review of each method, as well as its advantages and drawbacks, is presented.

2.1.2.1 Capacitive-Based Sensing

Capacitive sensors typically consist of pairs of plates whose capacitance is increased as the distance between opposite plates decreases or the permittivity of the dielectric

medium between the plates increases. Capacitive sensing is one of the most sensitive techniques for detecting small deflections of structures [15]. Its design is simple, with only two conductive parallel plates separated by a dielectric material. These plates are then isolated by an exterior material, like for instance an elastomer. When stretched or compressed, the material changes the geometry of the plates which causes a change in their capacitance [5].

For parallel plate capacitors, their capacitance can be given by 2.1.

$$C = \frac{A\varepsilon_0\varepsilon_r}{d}, \tag{2.1}$$

where C is the capacitance , A is the overlapping area of the plates, ε_0 is the permittivity of free space, ε_r is the relative permittivity of the dielectric material, and d the distance between plates [5].The change in capacitance can be measured, and in that way the force applied to the material that isolates the capacitor can be also measured. The force can either change the distance between capacitor plates or its area [16].

Figure 2.1 shows a capacitive tactile sensor and its working principle.

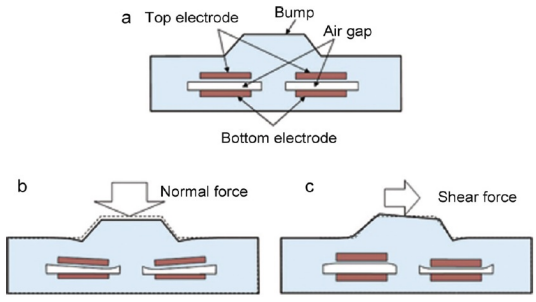

Figure 2.1: Illustration of a capacitive sensor and its response to normal and shear forces:(a) Cross-section view of a capacitive sensor with no applied forces; (b) response to normal forces; (c) response to shear forces. [15].

The change in capacitance can be measured by several conditioning circuits that will change according to the desired output signal. A current generator can be used to charge the capacitor for a fixed time interval. The output voltage will be proportional to the inverse of capacitance. Other circuits can use oscillators, whose running frequency depends on the capacitance. To have a correspondent voltage one can simply use a frequency-to-voltage converter [16].

This type of transducer principle is widely used due to the ease of fabrication of capacitor plates. Nevertheless, sensors that use this principle are more susceptible to noise, especially due to capacitive coupled interference when they are close to robotic metal parts [5] [16]. Good conditioning circuits can improve the quality of the voltage signals and reduce noise, to take advantage of the sensitivity achieved by some capacitive arrangements [16].

2.1.2.2 Piezoelectric-Based Sensing

Some materials, such as some crystals, ceramics or polymers generate a voltage potential, when deformed, that is proportional to the applied force or pressure. They can also work the other way around, having the ability to generate force when an electrical stimulus is applied. These properties grant them the name of *Smart Materials* [16] [5] [15]. Typically a piezoelectric sensor has the same configuration as the capacitance based sensors, although the dielectric material is now piezoelectric with a thickness t and area A. Usually in tactile sensors that use this transduction principle, the used dielectric material is a piezopolymer, which can be for instance Polyvinylidene fluoride (PVDF) [17]. This example is illustrated in Figure 2.2.

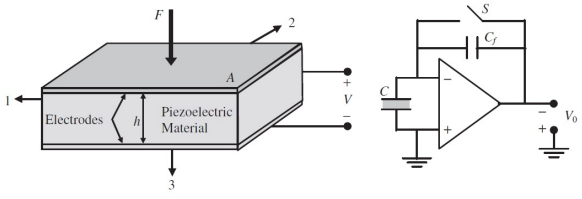

Figure 2.2: Piezoelectric based sensor and possible conditioning circuit [15].

Piezoelectric sensors exhibit a very good high-frequency response and are extremely sensitive having high voltage outputs even to small deformations [15] [5].

The conditioning circuit of these sensors is based on a ultra high input impedance amplifier, which can be seen on the right side of figure 2.2. Piezoelectric sensors are not adequate to measure static forces due to the high internal impedance of the piezoelectric films usually used in this technology.

2.1.2.3 Resistive-Based Sensing

Resistive sensors use the change in resistance of the sensing material to detect and measure forces. Most of the resistive devices adapt strain gauges as a sensing element, using the physical property of electrical conductance and its dependence on the conductors geometry. When the device suffers the action of a force, it causes strain that changes the geometry of the conductors and thus changes its electrical resistance. The applied force can then be determined by measuring the change in the electric resistance of the conductors [18].

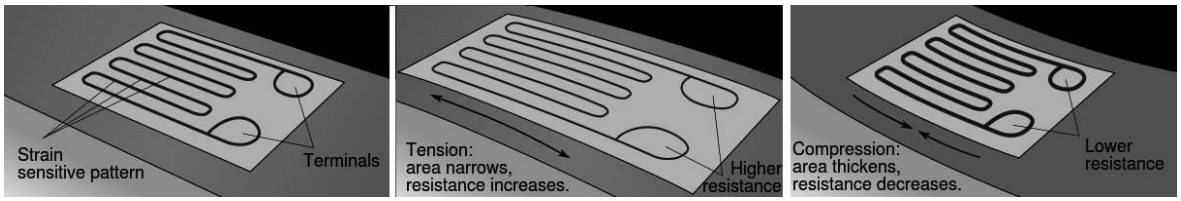

Figure 2.3: Illustration of the influence of tension and compression in strain gauges (Unknown Source)

.

Even though strain gauges are accurate, their substrate is often rigid. Stiff structures not only tend to provide low measurement sensitivity but also may not deflect even though a high force is applied [18].

Strain gauges are often used in a full Wheatstone bridge configuration in order to minimize temperature effects. If overloaded, they cannot be recovered. Their mechanical nature causes high hysteresis and non-linear responses. Nonetheless, the fabrication

methods and the best practices for their use are well established, which makes them one of the most used resistive sensing devices [19].

There have been some studies in which tactile sensors using flexible printed circuit boards (PCBs) have been developed for robotic applications. Even though this is a step forward in fighting rigid electronics, these sensors still have problems with adapting to joints since they do not stretch and exhibit fatigue on continuous bending.

Flexibility in electronics is a desired characteristic for many systems. With that feature it is possible to apply sensors to any kind of robotic parts, including joints, much like applying an artificial skin to those devices. This can be accomplished by elastomer-based sensing technologies, that are just recently being studied with deeper interest.

2.2 Soft Sensors and Electronics

Most of today's electronics are rigid, since they are fabricated on rigid substrates such as glass or polymeric materials [14]. This seems logical to provide them stability and durability. Nonetheless, rigid properties are not an advantage when adaptation to curvy/round objects is needed. Stretchability is even more important in robotics when there is a need to place sensors on joints or move parts of a robot. The sensor substrate needs to be extremely stretchable to adapt the twisting or bending behaviour of a joint, if that is the desired application.

Electronics that show good stretch abilities are expected to replace the traditional rigid electronics soon, since they can adapt to their host without inferring with its mechanical properties, and are highly deformable. The range of expectations and applications is wide, which makes the study of this kind of electronics extremely important.

Like in humans, a robot should be able to evaluate the properties of daily objects, so it can prevent failure in tasks that require manipulation [20]. The present project focuses on studying the application of stretchable electronics for soft and wearable sensing elements. Touch is important in everyday tasks, and the use of force and tactile feedback in robotics is now an active research topic involving multiple areas. Moreover, the goal is to obtain valuable information while minimizing the impact on the host, which implies the use of flexible and adaptive materials. A brief overview is now given to understand why these materials are so appealing to tactile sensing applications, and how they work.

2.2.1 Elastomer

There are three types of molecular arrangements that can result from a polymerization of monomers, namely glassy, crystalline and rubbery. An elastomer is a rubbery amorphous polymer which can expand or contract easily upon application of external forces. They have numerous cross-links that pull them back into their original form when the stress is removed. The cohesive interactions between the chains of an elastomer are week. Specifically, the weakness in the silicone-oxygen bonds, is what makes this amorphous polymer into a silicone with high elasticity [21] [22].

When deformed, a solid body has an internal reactive force called stress that resists to the deformation. Different materials have different ways to react to external forces. Figure 2.4 shows a stress-strain diagram for the three mentioned states of a polymer.

Stress can be defined as the force per unit area applied on a material, and strain its amount of elongation or compression relative to the original dimensions in the axis of strain [14]. A quick analysis of Figure 2.4 clarifies the benefits of using elastomers in stretchable electronics. Glassy polymers are hard and have no ability to suffer any major extensions. Cristalyne polymers go through successive changes.

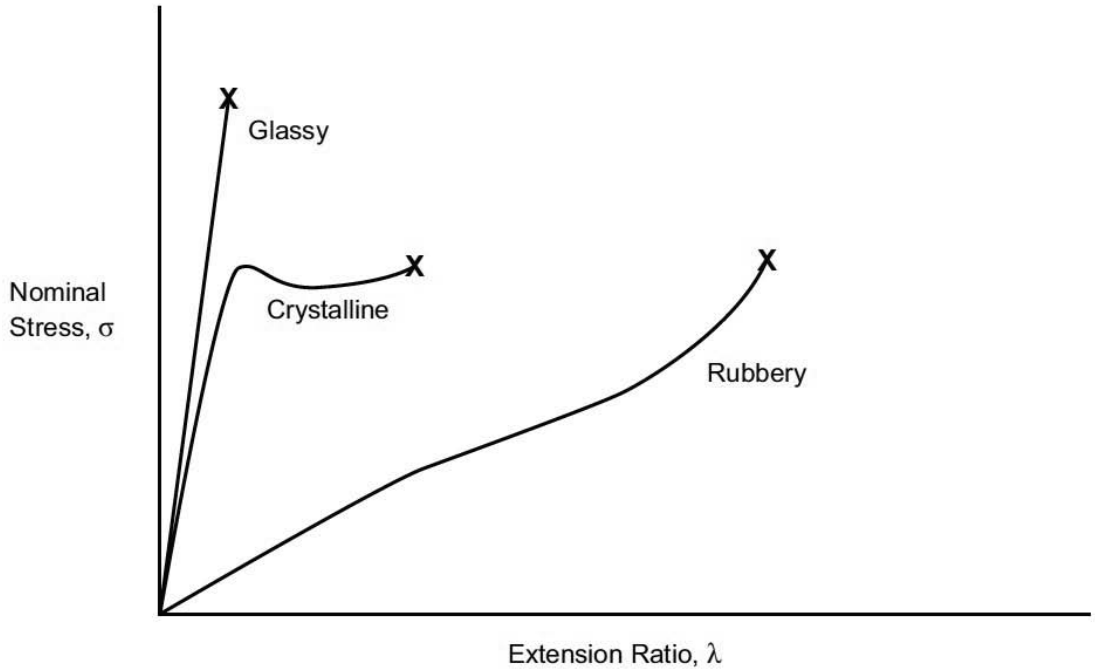

Figure 2.4: Strain-Stress diagram of three polymers in different physical states. The X marks the rupture point of the material [21].

They deform elastically, yield, deform plastically and fracture at last. Rubbers are unique, showing highly extensive elastic abilities and being also extremely soft. Their wide response to external influences such as pressure or strain and also their ability to change their shape under these conditions, turn silicone-rubbers into great engineering materials.

Nowadays there are a lot of commercially available elastomers with varying mechanical properties that meet specific needs of desired applications. The most common type of elastomers used by research groups in the area of stretchable electronics are silicone elastomers. They are basically polymers with low glass transition temperatures, which means that their transition from a hard state into a rubber-like state occurs at low temperatures [14]. The most common silicone-based elastomer is the polydimethylsiloxane (PDMS) since it is commercially available and has great mechanical properties [23] [24] [14] [25]. PDMS is optically clear, and, in general, non-toxic, and non-flammable. Its applications range from contact lenses and medical devices to elastomers.

Currently different types of soft sensors are being developed for force sensing. These devices are often employed as tactile sensors, which are primarily used to detect localized contact forces or strain.

Regardless the type of force sensor, the elastomer is the first element in the transduction of pressure or strain, since the deformation of the material is what is detected and transduced into an electrical signal to be read by appropriate electronics. Current elastomeric tactile sensors can be classified into piezoresistive, piezoelectric and capacitive.

Soft sensors are a recent area of interest. Commercially available sensors, which are frequently rigid, do not fill the needs of wearable electronics, soft robots or human-machine interaction systems. The formulation of sensors made of soft materials, like elastomers, can give valuable sensing information and minimize the impact in the mechanical properties of a possible host.

Here a review of different technologies developed through the years is presented. Since this is an emerging technological area, a lot of different formulations are presented, and so this overview will be organized by type of transduction principle of the developed device.

2.2.2 Soft Resistive Sensors

2.2.2.1 Kramer et al. (2011)

Kramer et. al [26] stated that elastomer-based sensors, artificial skin and MEMS represent a step forward in progressing from rigid to soft electronics. This research group used the principle of liquid embedded elastomers to introduce resistive stretchable sensors that measure curvature. That formulation was basically a sensor composed of two elastic films connected along their edges and in the middle by a strut, a struc-

tural component designed to resist longitudinal compression. One of the layers has a channel filled with conductive metal (EGaIn) which is placed over and along the strut.

The suggested curvature sensor is shown in figure 2.5.

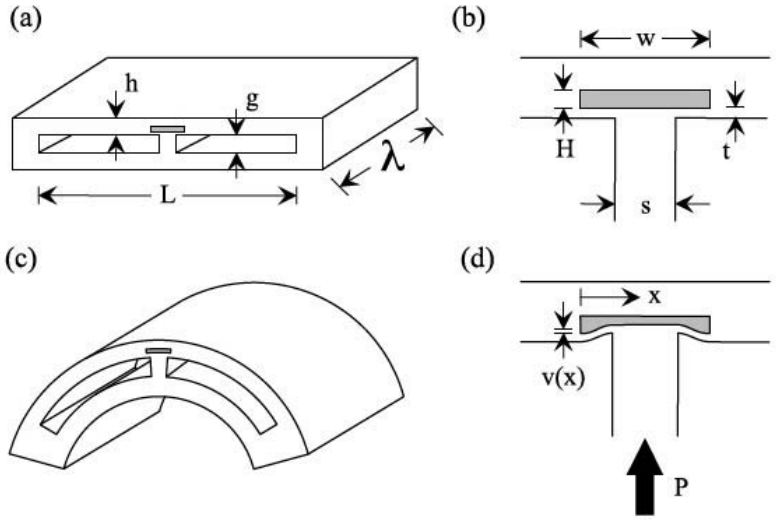

Figure 2.5: Curvature Sensor:(a)The sensor includes two layers with lenght L, thickness h, width d and with a gap g. (b) The strut s has a microchannel placed above it, with height H and width w at a distance t from the strut. (c) When the sensor is bended a compressive force is induced. (d) The compressive force P causes the embedded channels to deform [26].

When pressure is applied to the sensor, it induces a compressive force in the strut s, that causes the cross-section of the channel to deform, which leads to a change in electrical resistance. The bending curvature is then determined by measuring the electric resistance change.

The functionality of the developed sensor was later demonstrated by testing it on a finger joint. Stretch, pressure and curvature sensing were combined to introduce a family of wearable soft sensors that could detect bending and joint position. The sensor was wrapped around a finger joint, specifically with its sensing element on the middle knuckle of a finger. When the finger bended it stretched the elastomer and pressure was exerted on the sensing element. The principle of resistance change is applied again [27].

The developed sensor was calibrated on and off the finger. An exponential relationship between bending angle and change in resistance was found, and fitting the obtained exponential curves to the collected data allowed to establish the relation given by 2.2 [27]:

$$\theta = \frac{1}{b} \log(\frac{\Delta R + A}{A}) \tag{2.2}$$

After comparing the actual and predicted curvature angle of the joint, Kramer et al. obtained consistent results, that proved that the designs developed by the group were viable for the desired application. Figure 2.6 shows the developed sensor wrapped around a finger joint, illustrating one of the possible applications of the developed device.

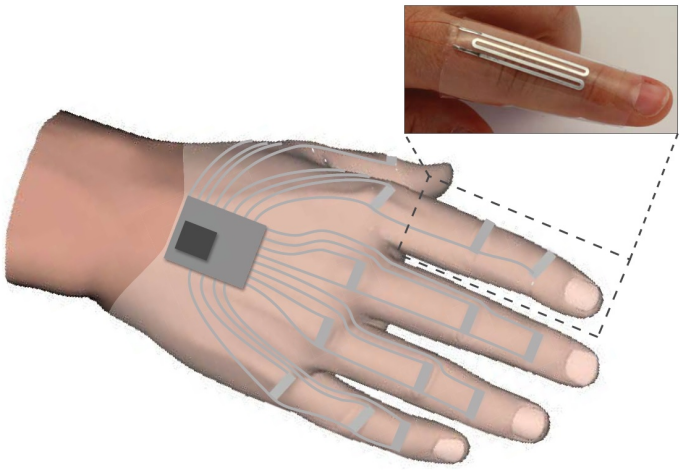

Figure 2.6: Illustration of curvature sensor wrapped around every finger of a human hand. In the detailed view an actual sensor is placed on a human finger joint [27].

2.2.2.2 Hammond et al. (2012-2014)

Hammond and his research group presented soft tactile sensor arrays for micromanipulattion [28]. The fact that micromanipulation is an essential capability in advanced procedures in medicine motivated the work of these researchers. In medical procedures, handling delicate structures such as surgical instruments or compliant biological tissues requires sensing feedback and modulation of the applied forces to prevent unwanted damage. A soft tactile sensor array with sub-millimeter resolution was designed and experimentally validated for application in micromanipulation. The sensor had conductive liquid-filled microchannels embedded on an elastic body, that when deformed by compression or stretching induced a change in its electrical resistance.

Taking performance requirements for demanding microsurgery tasks, the sensor was designed and the deformation of its microchannels was simulated. Knowing the cross-sectional area of a rectangular microchannel and the electric properties of the conductive liquid within, the change in the electrical resistance of the microchannel due to pressure was found to be:

$$\Delta R = \frac{\rho L}{wh} \left\{ \frac{1}{1 - 2(1-\nu^2)wp/Eh} - 1 \right\}, \tag{2.3}$$

where ΔR is the change in resistance, ρ is the electrical resistivity, L is the length of the microchannel, w its width and h its height. p is the contact pressure, and ν and E are the Poisson's ratio and the elastic modulus of the material, respectively. Figure 2.7 shows the overall sensor morphology:

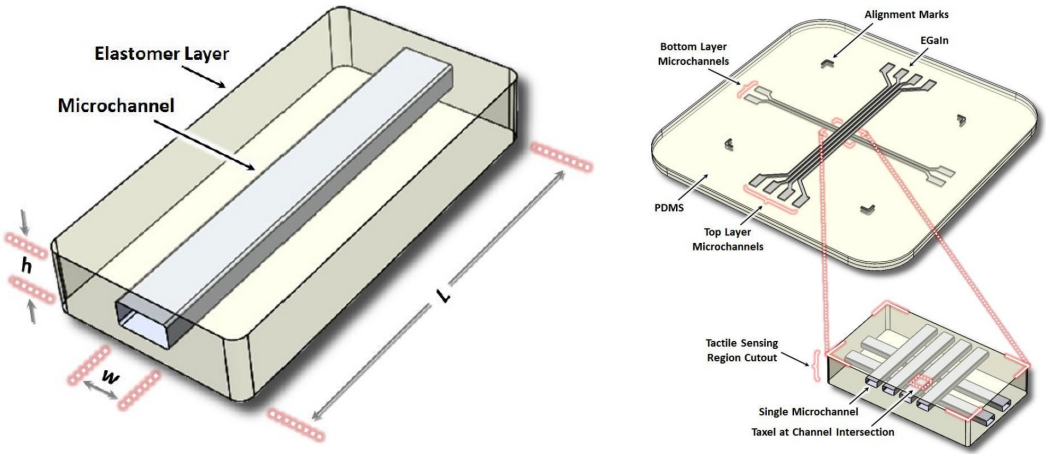

(a) Drawing of a conductive liquid filled microchannel embedded in the elastomer [28].

(b) Overall sensor morphology developed by Hammond et al.

Figure 2.7: Comparison between the channels geometry studied in [28] and the one adopted for the present project

This design intended to detect contact with sub-millimeter resolution and sense forces of 10's of milli-Newtons; A simulation was also conducted to test if the sensor geometry fitted the performance requirements for demanding microsurgery tasks. A prototype was then made and tested to characterize performance of the sensor and validate the design. Even though the efforts to design a good device proved to be efficient, the designed sensor was then improved due to mismatches between sensor layers and limited functionality for high loads/pressures [29].

2.2.2.3 Park et al. (2010-2013)

The work of Dr. Park is motivated by the idea that next emerging technologies in robotics will depend on stretchable sensors that are able to register deformation and surface pressure. The first presented hyperelastic device designed by Parker et al. was adapted from the Whitney strain gauge, introduced in 1949. This device was composed of a rubber tube filled with mercury and used a Wheatstone bridge to measure the change in electric resistance of the mercury, that matched the stretch of the material [30]. In fact the group presented more than one hyperelastic sensor: 3 sensors

with dimensions greater than 250 μm, and 1 with dimensions between 20 and 300 μm. The first three were fabricated by casting uncured silicone rubber on 3D printed molds. After curing under ambient conditions two elastomer layers were bonded together, one with engraved microchannels and one with a flat surface. A syringe was used to fill the assembly with a liquid metal.

The fabrication of the sensor with smaller dimensions consisted of casting liquid-form PDMS elastomer in a mold patterned by soft lithography. In both formulations the action of a pressure force to the surface of the elastomer, induced the deformation of the underlying microchannels, changing their electrical resistivity. Pressures in the range of 0-100 kPa were measured with a 1 kPa resolution, and for that range the resistance changed as much as 50 percent its original value. The presented sensors are shown if figure 2.8 in which the geometry of the microchannels and their arrangement and dimensions are perceptible.

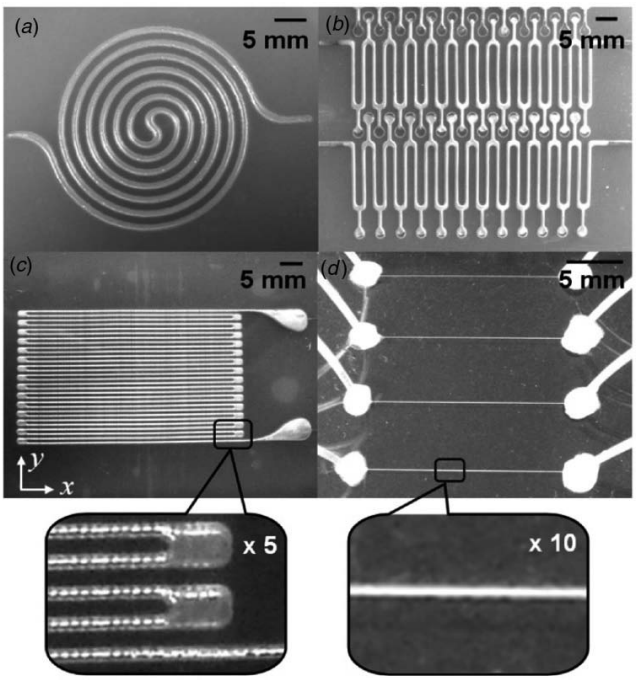

Figure 2.8: Thin polymeric layers embedded with microchannels of conductive liquid. (a)-(c) Uncured Ecoflex® cast from 3D printed molds with channel heights and widths of 1 mm, 750 μm and 300 μm, respectively. (a) is intended for pressure sensing only while (b) and (c) are intended for strain sensing. (d) Embedded PDMS microchannels fabricated through soft litography with 20 μm height and different widths from 25 to 40 μm.

This work was later applied to a soft wearable sensing suit, developed for complete body motion sensing with minimal complexity [9]. One of the key elements of the suit was the previously mentioned hyperelastic sensor, namely the strain one, visible on figure 2.8 c). The suit represented a useful tool to understand the biomechanins of the human body.

Dr. Park and his research group proceeded with the study of hyperelastic sensors. The next step was to develop an artificial skin so that robots could turn into more autonomous machines and devices. The group presented an artificial deformable skin that provided multi-modal sensing capabilities [31] [32].

The fabrication process is the same as the one for developing the hyperelastic strain sensors showed in figure 2.8 a) and c). Even though, in this new project 3 layers were casted from 3D printed molds, having interconnected points so that the layers could always be in contact. The skin was able to detect and distinguish between three different stimuli: X-axis strain, Y-axis strain and Z-axis pressure. The first two layers had parallel channels, much like in strain gauges, designed to detect X/Y-axis strains. The third layer had a circular pressure intended to detect pressure.

The finished prototype of the artificial skin had an overall size of $25mm \times 25mm$ and a thickness of $3{,}5mm$. The channels had 200 μm of width and a height of 300 μm. The sensor remained functional up to strains of approximately 250 percent of its characteristic modulus, and his shown in figure 2.9.

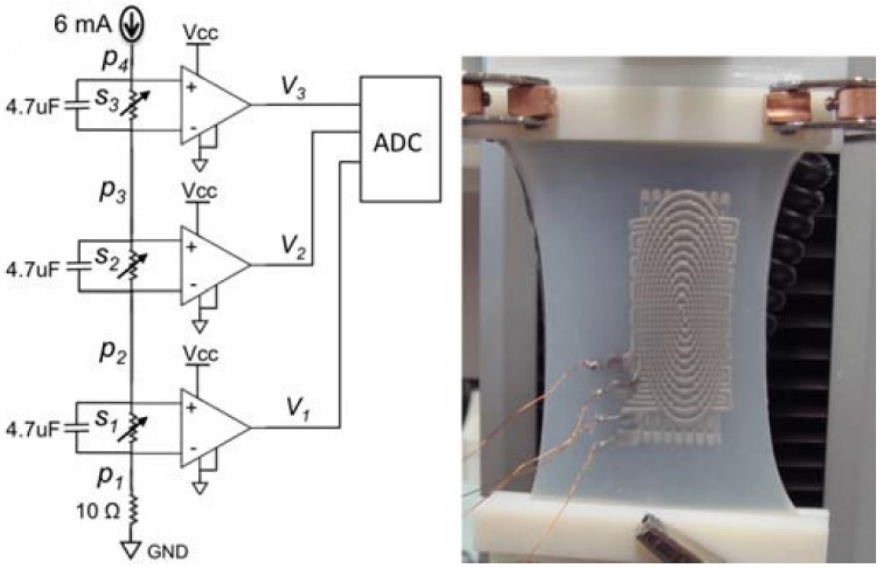

Figure 2.9: Final artificial skin developed by Park et al. and example of conditioning circuit: The final sensor is submitted to strain in an exemplifying calibration process. The diagram to the circuit used to read the sensor signals is also presented [31].

It is interesting to mention that in the entertainment industry motion suits like the one developed by Park et al., and mentioned in the Introdcution of this project, are used to measure motion of the wearer and puppet a computed generated avatar. This proves once again the broad application field of technology involving soft sensors. Applications of the work developed through the years by Park et al. may include either, humanoid robotics, wearable robotics and medical robotics. For the last one this group developed several sensors for application in soft wearable assistive robots, like the work presented in [8] [3] [10].

2.2.3 Soft Capacitive Sensors

2.2.3.1 Ulmen et al. (2010)

The increasing of human-robot interaction leads to a need for safety on robotic platforms. Safety implies that robots must be more responsive to unexpected contact anywhere on their parts than most of traditional robots. The work presented by Ulmen et al. introduced an artificial skin that not only absorbs energy in unexpected collisions but also is available for different sensor areas and populations due to its low-cost fabrication methods [33].

The designed device was also intended to be adaptive to curve and compliant surfaces, be mechanically robust and present low electrical and stray capacitance noise. The sensing element in the presented artificial skin is a force sensing capacitor. The sensor consists of layers of foam, since in general they have desirable properties to absorb energy in collision even though they present high hysteresis. Shielding the sensor provides immunity to both electrical noise and stray capacitance effects. Figure 2.11 shows the proposed sensors and its different layers.

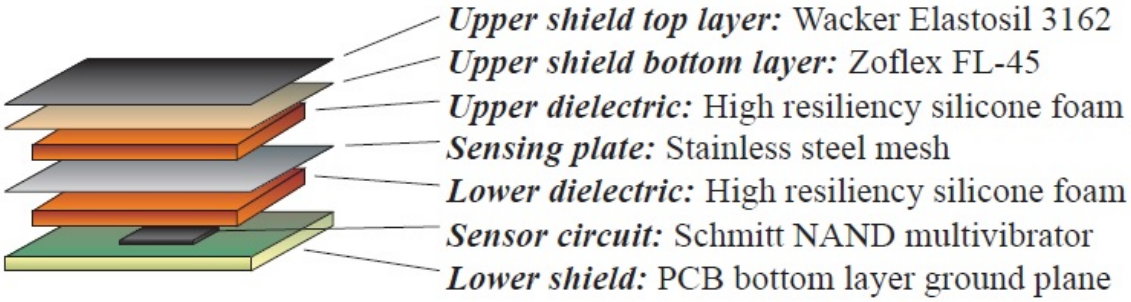

Figure 2.10: Layer structure of the three plate capacitor used by Ulmen et al. [33].

A 4 × 4 array was constructed, with multiple of the small previously illustrated sensor. The sensor components were first mounted to a PCB, to which flexible conductive plates were attached to form the sensing plates of each sensor. There was a dielectric layer on the bottom the PCB that acted as the lower shield. Then a layer of dielectric silicone foam was bonded to cover all components. At last, a foam layer coated with conductive rubber was bonded to the top of the array. The outer conductive layers of the capacitors worked both as plates and noise shields. A small circuit was placed in each taxel, which also minimized noise since the digitization was immediate.

This work can be improved if the rigid PCB is replaced by a flexible one. That substitution will allow the sensor to be wrapped for instance around surfaces.

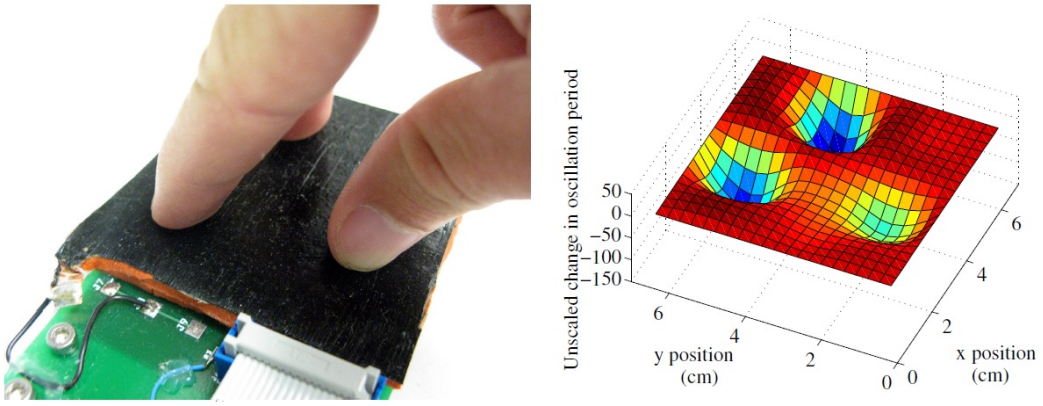

Figure 2.11: Tactile display recorded from the developed 4x4 capacitive array [33].

2.2.3.2 Ponce et al. (2012)

Motivated by the fact that in most cases visual and acoustic feedback do not provide the necessary information for decision making, Ponce et al. presented a flexible capacitive microfluidic sensor for normal force sensing [19]. The sensor was fabricated by soft lithography and consisted of two main materials: PDMS to mimic the properties of human skin and a liquid metal namely Gallistan (EGaIn), to serve as flexible plates for the capacitive sensing unit. The outer layers of PDMS contained the microchannels filled with the conductive liquid-metal and the inner layers sealed the microfluidic layers.

The developed sensor showed reliable results for forces up to 2,5 N and exhibited 0,5 mm spatial resolution. When wrapped around a surface with low curvature it remained functional, even though the group considered that the prototype was not adequate to provide a good force analysis to artificial hands, one of the envisioned applications. The developed prototype is visible in figure 2.12.

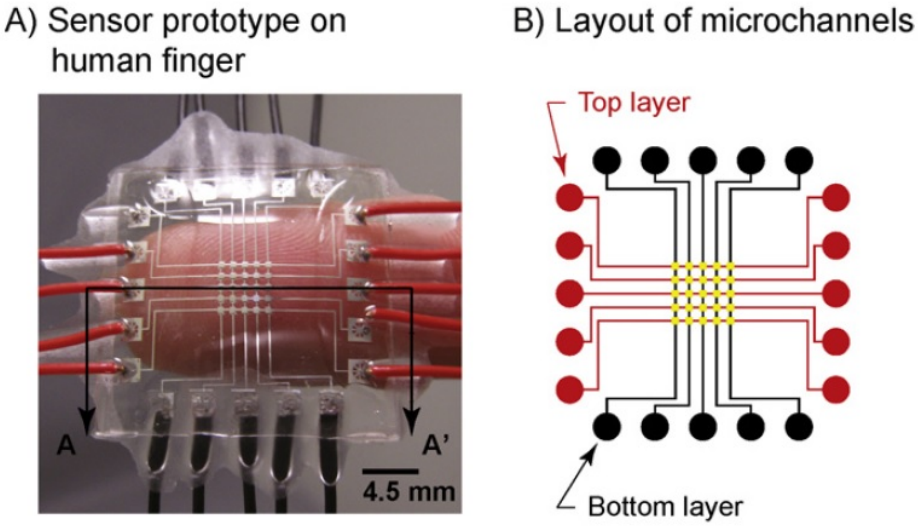

Figure 2.12: Prototype for capacitive microfluidic artificial skin. (A)embedded EGaIn in the polymeric material. (B)two microchannel paths in the two different layers of the artifical skin (black and red) [19].

2.2.3.3 Roberts et al. (2010-2013)

In tactile sensing, fabricating shear force sensing devices was in general challenging. Robert et al. designed a promising sensor that consisted of a thin-elastomer film embedded with a liquid phase EGaIn alloy, that registered elastic shear and pressure [34].

The sensor consisted of four fluidic capacitors that shares a square shaped electrode. The parallel plate capacitors were embedded in sheets of Ecoflex® 0050, previously used in elastomer based sensors. Alongside the dielectric material, in other words the middle layer of the sensor, was fabricated from Ecoflex® 0010 . Needle injection of the conductive metal, the method used in [30] [31] [32] was avoided by using a masked deposition method followed by a freezing technique to solidify the metal alloy and create the planar electrodes, i.e the capacitor plates.

Shearing the surface of the sensor caused the electrodes to slide past each other, changing their capacitance, which also happened when pressure was applied. The sensor was able to detect shear displacement in two directions in the range of -3 mm -3 mm

with a resolution of 500 μm, and pressure up to 25 kPa with 5 kPa resolution. The developed work still needs evaluation for wearable electronics and robotic manipulation, considered as future work for Roberts et al. The developed prototype can be visualized in figure 2.13.

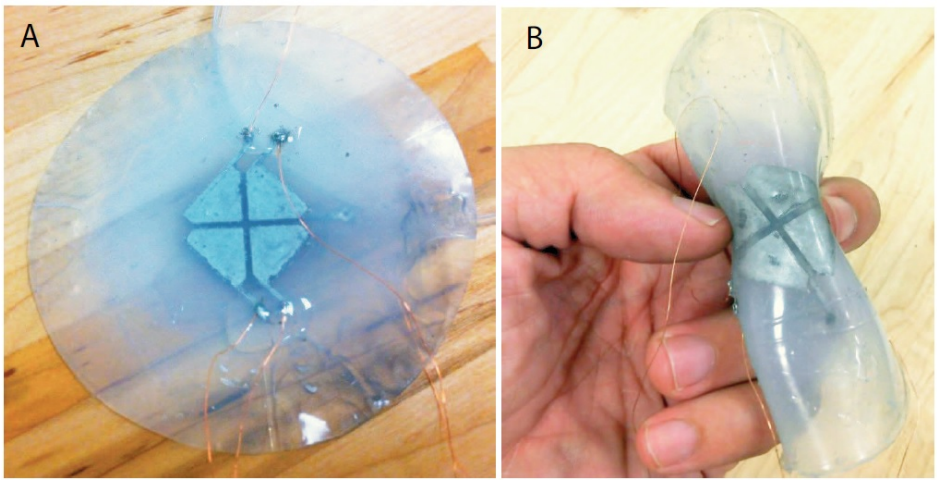

Figure 2.13: Shear sensor presented by Roberts et al. :(A) The developed soft-matter shear sensor. (B) Demonstration of the ability of the sensor to stretch and bend with no restrictions [34].

Significant progress has been made in the area of skin-like sensors through the last four years. However, each type of sensor has different trade-off when it comes to sensor performance, complexity and cost.

The use of low-cost soft organic materials in circuitry is an exciting advancement in the field of tactile sensors.

Chapter 3

Methods and Materials

This chapter describes the entire fabrication process, including the design and all the steps towards finding the appropriate fabrication conditions and parameters. Specifically the Methods in this project include:

- Design and 3D printing techniques for the fabrication of the molds.
- Fabrication of the sensors:

  Casting of the silicone.

  Bonding of the cured silicone layers.
- Injection of the liquid metal alloy in the fabricated and sealed sensors.

The diagram in figure 3.1 is intended to provide an overview of the fabrication process of the sensors in order to clarify all phases and make them easy to understand for the reader of this dissertation.

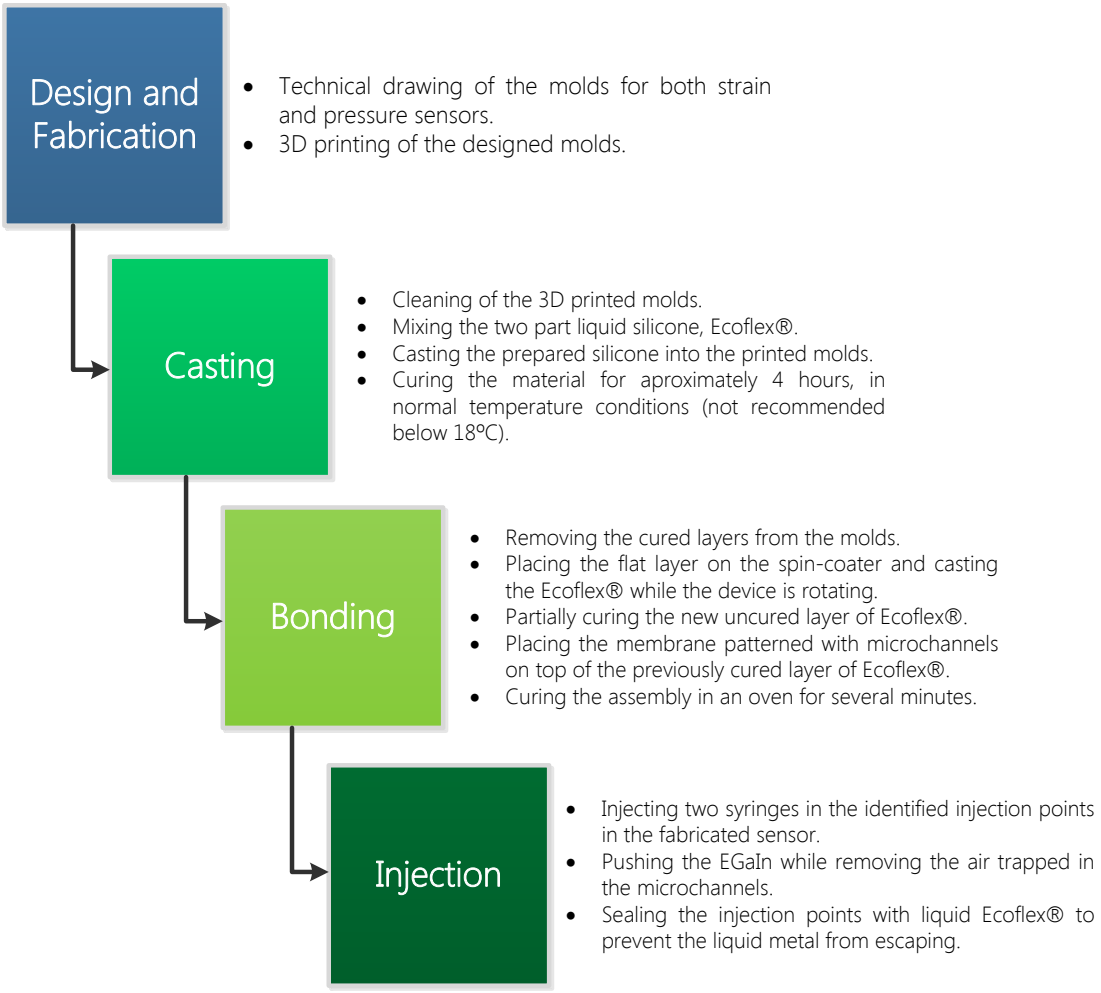

Figure 3.1: Global fabrication steps for both strain and pressure sensors.

Soft sensors are recent technology and even though the investigation on this subject is increasing, there is still a great space for study and improvement. This work does not aim to go further than the presented State of Art. At this stage it aims to expertise one of the fabrication processes presented in Chapter 2 and accomplish that with low cost methods.

The use of 3D printed molds to engrave the channels on the silicone-rubber turns the process low cost and accessible in comparison to other technologies, such as soft lithography.

The used silicone-rubber has great mechanical properties and is easy to manipulate, which can turn the fabrication of soft sensors into something less demanding. Nonetheless the dimensions of the fabricated sensors are small, with dimensions in a μm scale. This requires not only a careful study of each used material and process, but also good fabrication techniques.

The fabrication of the sensors is adapted from an artificial skin formulation with embedded microchannels [30] [9], mentioned in the state of art, that can be visualized in figure 3.2.

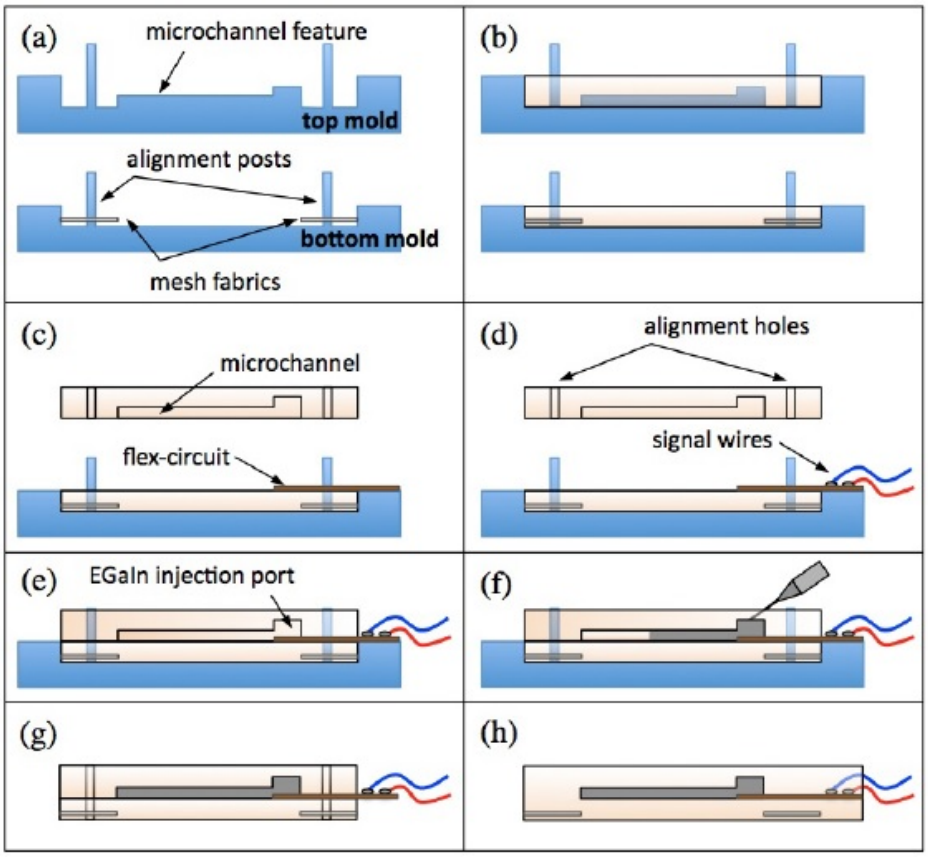

Figure 3.2: Fabrication of a soft sensor proposed by Park et al. (a) Prepare molds (3D printed). (b)Pour liquid silicone. (c) Remove top mold and place flex-circuit on the bottom layer with alignment. (d) Solder signal wires on the flex-circuit. (e) Bond the top layer to the bottom layer. (f) Inject EGaIn. (g) Remove bottom mold. (h) Final sealing for wire protection. [9]

The artificial skin presented by Park et al. was made using a three step process that included casting, bonding and metal injection as shown in figure 3.2.

3.1 Design

The goal of this work was to replicate the process showed in the figure 3.2, in order to develop two different soft sensors, one for strain sensing and other for tactile sensing. The designed molds are intended to engrave microchannels in a stretchable material that can be filled with conductive metal. The fabrication of the sensors begins with the first draft of the molds, and to have a good design it is important to evaluate the right geometry of the channels and their right profile and dimensions first. The first idea of application for the soft sensors was the adaptation to the fingers of a robotic hand. Therefore the dimensions of the sensors were limited, based on the fingers prototypes.

One of the drawbacks of this kind of technology is the sensitivity of the sensors. A research group from Harvard University in Cambridge studied the influence of cross-sectional geometry of the channels in the sensitivity of pressure sensors [35]. Their work proposed a solution to improve sensors sensitivity by changing the physical geometry of the embedded microchannels. Based on these considerations, the profile chosen for the microchannels was a concave triangular geometry, since it seems to exhibit most linear responses to pressure and least amount of hysteresis.

Three different designs were developed, one for tactile sensors and two for stretchable strain sensors. In both cases two molds for each sensor were designed, one with a flat surface and another with embossed microchannels. The cross section of the channels was designed to be similar to a concave triangle, constrained only by the limitations of the 3D printer. These limitations forced the cross section to be concave with a rounded top instead of triangular. Figure 3.3a shows the geometry proposed by the Harvard Research group and figure 3.3b shows the geometry of the microchannels for the sensors developed in this project.

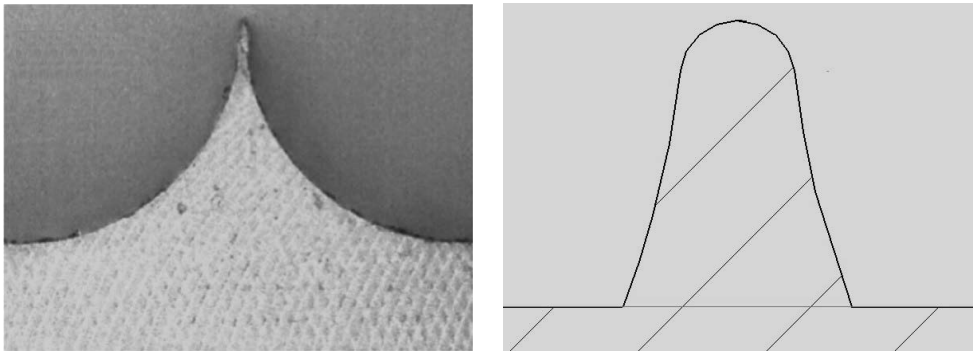

(a) Microchannel with concave triangle cross section [35].

(b) Cross side of the sensors in this project

Figure 3.3: Comparison between the channels geometry studied in [35] and the one adopted for the present project

A description and an illustration of the different designs follows in the next topics.

3.1.1 Strain Sensors

For strain sensing, the design should ensure that when the material suffers strain in the axial direction of the channels, the overall channel length and cross sectional area are changed. That change should modify the electrical resistance of the channels [31]. Figures 3.4-3.6 show the three different designs for the developed strain sensors, with specified dimensions in milimeters (mm). Based on the design of strain gauges, that are the most common resistive-sensing devices, parallel channels with a width as low as 400 μm were designed.

Figure 3.4a shows the technical drawing of the top view of the first designed mold. The mold has 47,70 mm of width and 29 mm of length, with only 17,70 mm for the channels arrangement. This leaves enough space for connection points to test the sensor further ahead. The microchannels have 0.8 mm of width, 12,50 mm of length (3.4a) and a height of 1 mm, as detailed in figure 3.4b. In that figure it is also visible that the width decreases as one reaches the top point of the channel, to reproduce the design of the channels introduced in [35].

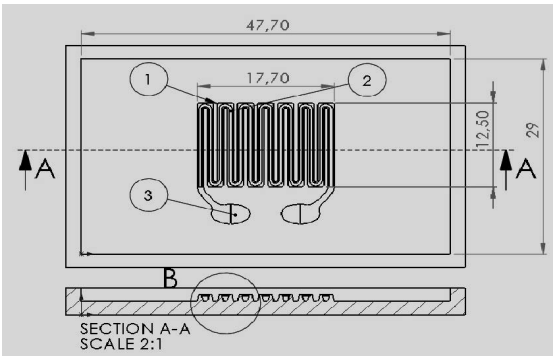

(a) Drawing of the mold for the strain sensing sensor; Section A-A shows a section view of the mold with a 2:1 scale.

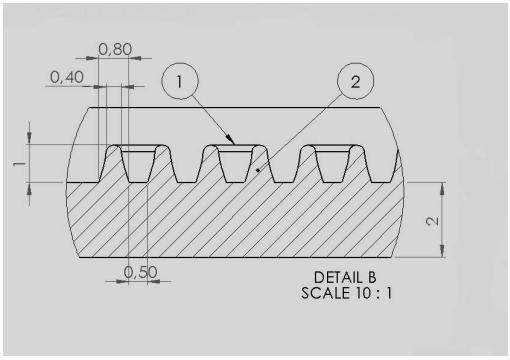

(b) Detailed view of Section A-A, showing the cross section profile of the microchannels.

Figure 3.4: Strain sensor with conic cross sectional channels of 0.8 *mm*.

The numbered balloons in both 3.4a and 3.4b, intend to establish a correspondence between the two different views of the design. 1 is the link between two adjacent channels and 2 is a microchannel.

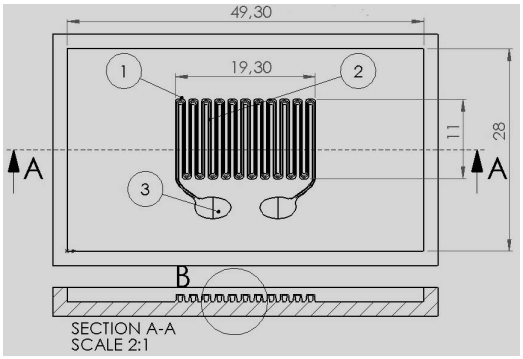

(a) Drawing of the mold for the strain sensing sensor; Section A-A shows a section view of the mold with a 2:1 scale.

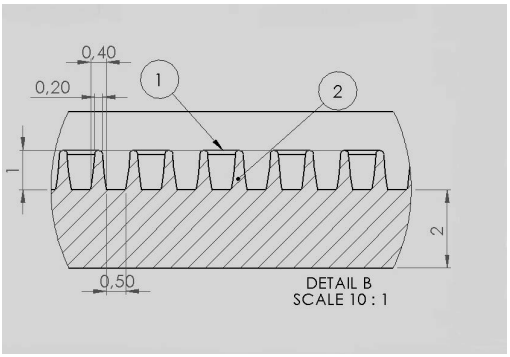

(b) Detailed view of Section A-A, showing the cross section profile of the microchannels.

Figure 3.5: Strain sensor with conic cross sectional channels of 0.4 *mm*.

Figure 3.5 shows the technical drawing of a mold similar to the previous one. Since this technology is still recent, this second design aims to project smaller channels within the dimensions established for the first mold. Figure 3.5a shows the 2 dimension draw of the top view of the second designed mold. The mold has 49,30 *mm* of width and 28 *mm* of length, with only 19,30 *mm* for the channels arrangement. In figure 3.5b the dimensions of the channels are specified. They have 0.4 *mm* of width, 11 *mm* of length (3.5a) and a height of 1 *mm*. The numbered balloons in both 3.5b and 3.5a

establish the correspondence between the two different views of the design. 1 is the link between two adjacent channels and 2 is a microchannel.

The injection points identified in the figures 3.4 and 3.5 with the number 3, are intended to have larger dimensions so that a syringe can be easily placed to inject the liquid-phase metal. There are two injection points, one to inject the liquid metal and other to remove the air trapped in the channels.

In this version efforts to be less conservative in terms of the channels width were made. Embedding channels in a small space is advantageous when it comes to the overall size of the final sensor. However at first it was not clear if it was possible to fabricate the molds, and the sensor itself, with such small dimensions. The main concern was the proper printing of the designed molds, and the sealing of the sensor. For this reason two versions of the strain sensors were designed at first trial, and after a valid fabrication of the devices, with satisfying results, a small mold was designed some months later.

Figure 3.6a shows the technical drawing of the top view of the third designed mold. The new mold has 49,30 mm of width and 28 mm of length. In figure 3.6b the dimensions of the channels are specified. They have 0.6 mm of width, 14 mm of length (3.6a), a height of 1 mm and are separated by 0.6 mm. This smaller design allows the integration of the sensor in the joint of the fingers for the ISR-Softhand.

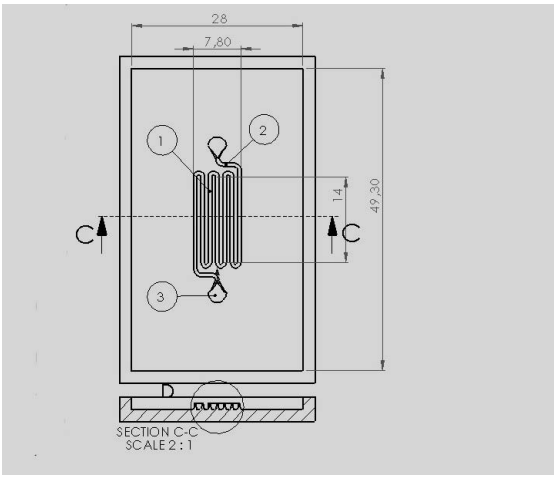

(a) Drawing of the mold for the strain sensing sensor; Section C-C shows a section view of the mold with a 2:1 scale.

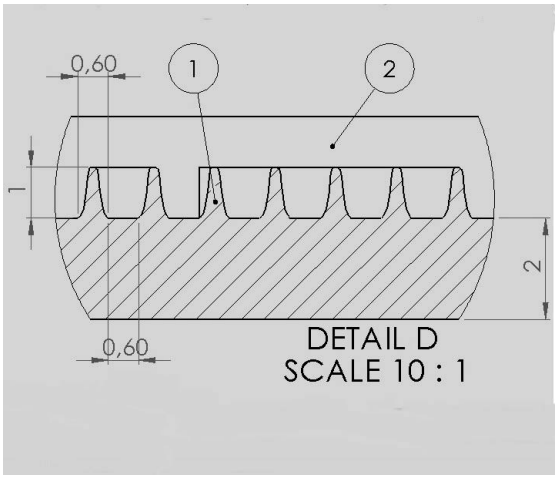

(b) Detailed view of Section C-C, showing the cross section profile of the microchannels.

Figure 3.6: Strain sensor with conic cross sectional channels of 0.6 *mm*.

3.1.2 Tactile Sensor

For pressure sensing, the design should ensure that when pressure is applied to the surface of the elastomer, the cross-section of the embedded liquid-phase metal channels deforms and the electrical resistance of the channel changes [35]. Figure 3.7 shows the designed pressure sensor with specified dimensions in *mm*.

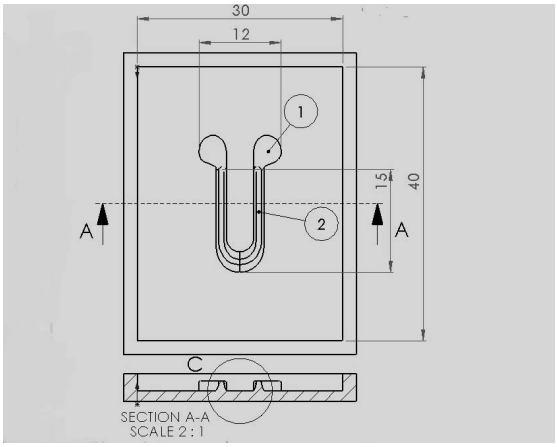

(a) Drawing of the mold for the pressure sensing sensor; Section A-A shows a section view of the mold with a 2:1 scale.

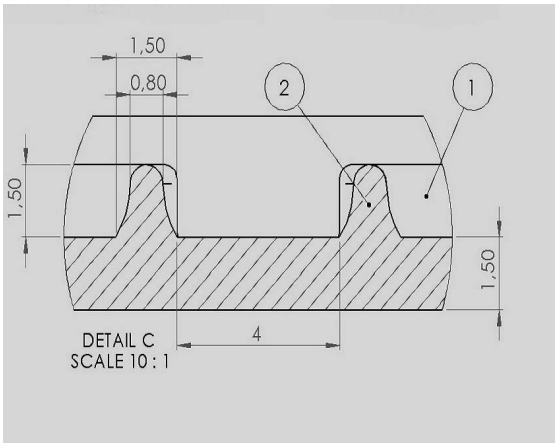

(b) Detailed view of Section A-A, showing the cross section profile of the microchannels.

Figure 3.7: Pressure sensor with conic cross sectional channels of 1.5 *mm*.

Figure 3.7 shows the draw of a mold for pressure sensing sensors. Figure 3.7a shows the 2 dimension draw of the top view of the designed mold. It has 30 mm of width and 40 mm of length, with only 12 mm for the channels arrangement. In figure 3.7b the dimensions of the channels are specified. They have 0.4 mm of width, 15 mm of length (3.7a) and a height of 1 mm. The numbered balloons in both 3.7b and 3.7a establish the correspondence between the two different views of the design. 1 is one of the injection points and 2 is a microchannel.

This sensor is intended to be placed on finger pads, and so its dimensions must be limited.

Figure 3.8 shows the technical drawing of the flat molds designed for the fabrication of flat membranes that are intended to isolate the microchannels in the patterned ones.

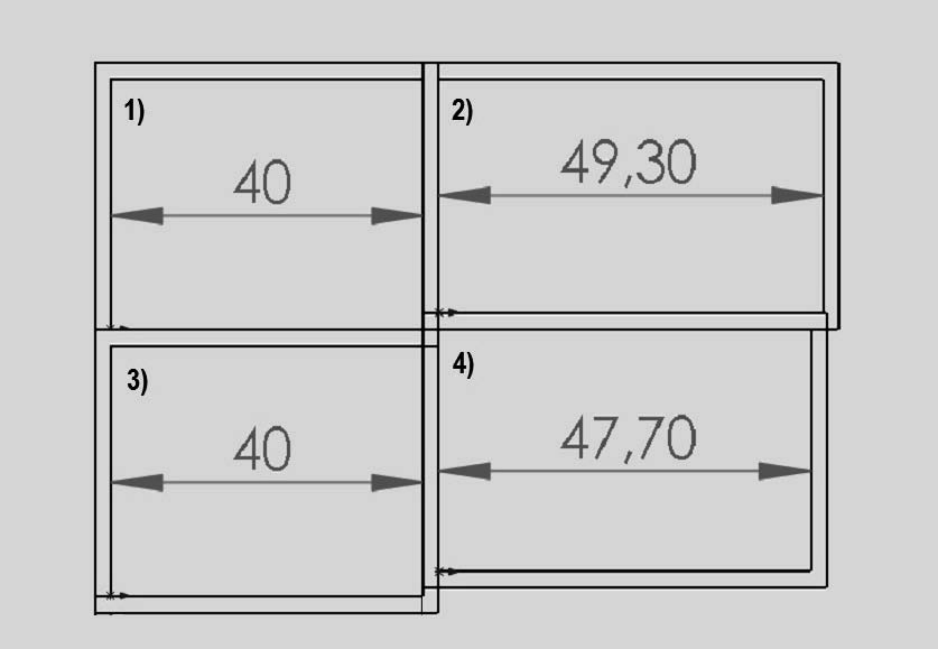

Figure 3.8: Drawing of the flat molds for the 4 different flat layers that match the 4 different sensors.

In figure 3.8, **1)** and **4)** match the mold visible in figure 3.7, **2)** the molds in figures 3.5 and 3.6 and **3)** the mold in figure 3.4.

It should be noted that all previous designs were made to fit the capabilities of the 3D printing equipment that was chosen for this project. This will be further described in the following section.

To simplify the identification of the molds, the one designed for strain sensors will be called strain-sensor mold, and one for fabricating pressure sensors will be called pressure-sensing mold.

3.2 3D Printed Molds

The purpose of this section is to provide an overview to the 3-D printing technology, selected for the making of the previous detailed designs.

3.2.1 3D Printing Technology

3D printing is a growing technology for low cost rapid prototyping of objects. Through a series of cross-sectional slices a 3D printer is able to create a 3D structure on a layer-by-layer method. As 3D printing technologies evolve, fabrication costs decrease and the properties of the manufactured objects become better. The time saved in product development, freedom of design and fabrication with no need for tools can reduce significantly the fabrication costs per item [36]. Figure 3.9 resumes some characteristics of 3D printing technology.

3D modelling softwares such as Solidworks or Inventor enable the design of a product with the desired and specified characteristics and its exportation to a printable format.

There are several technologies for 3D printing of different materials, with different requirements in terms of functionality, tolerance, minimum feature, size or finishing. The most common are Stereolithography (SLA), Selective Laser Sintering (SLS) and Fusing Deposition Modeling (FDM).

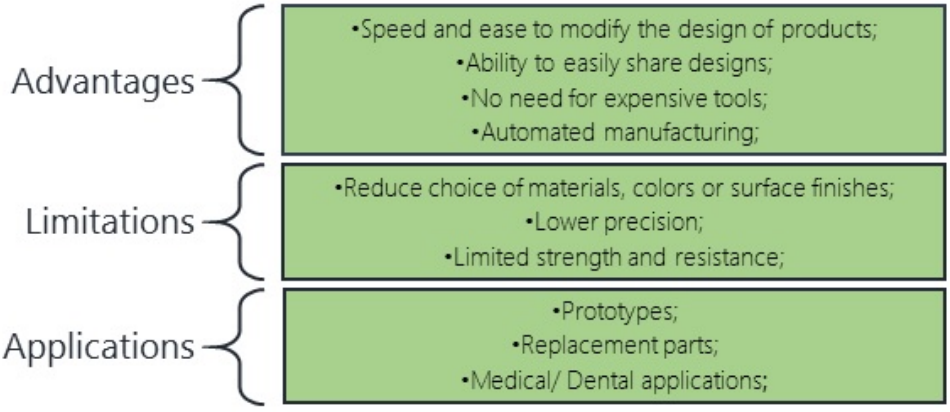

Figure 3.9: Resumed advantages, limitations and applications of 3D printing technology.

Figure 3.10 gives an overview of the 3D printing methods mentioned previously, followed by a brief description of each technology.

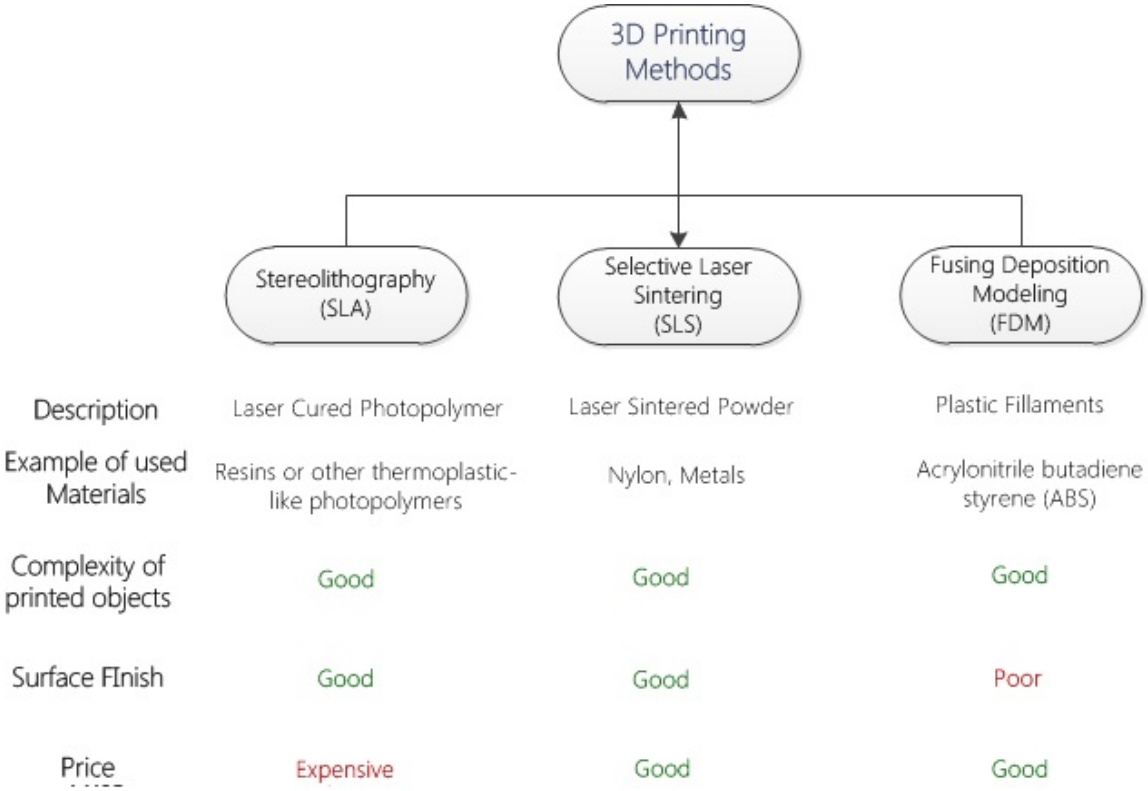

Figure 3.10: Overview of different 3D printing methods.

3.2.1.1 SLA

SLA is a manufacturing process that creates a 3D structure by superposition of liquid photopolymeric resin layers. According to the design of the object, an UV (ultraviolet) laser solidifies the curable photopolymer resin layer by layer, following the contours of the desired object. For each layer the laser traces a cross-section of the desired pattern on the surface of the liquid resin. When exposed to the ultraviolet laser light, the resin cures and the traced pattern solidifies. The remaining resin is removed by heating in an UV oven. SLA can produce parts with complex geometries and excellent surface finishes when compared to other processes [36]. In fact SLA has been used to fabricate molds for the preparation of implants in cranial surgery, and to develop patient-specific implantable devices. This is a curiosity that sustains the wide applicability of this 3D printing technology.

3.2.1.2 SLS

SLS is a manufacturing process that uses a laser to build parts by fusing powdered material layer by layer from the bottom up. It is possible to fabricate accurate and durable parts with SLS, but the finish is relatively poor with a grainy or sandy feel. The most used material for this purpose is Polyamide (PLA), also known as Nylon. The overlapping layers are chemically bonded by the action of temperature from a laser emission equipment. The process begins with the deposition of a thin powder layer within a cylinder that gives form to the designed object. This superposition process is repeated until the whole object is formed. The powder that failed to be laser sintered is removed after the part is complete. Since there is reduced strength between the fused particles the fabricated parts tend to be weaker even though complex geometries can be obtained [37].

3.2.1.3 FDM

The FDM process builds parts by extruding polymeric filaments such as Acrylonitrile Butadiene Styrene (ABS) and PLA, from the bottom up, through the use of a computer controlled print head. The device machine selectively re-melts and deposits the filaments on the prior layer for each cross section of the desired part. FDM parts tend to be stronger due to the use of ABS, a rigid lightweight and thermoplastic material with some flexibility and strength in terms of impact absorption. Nonetheless, the fabricated parts are sometimes porous and have a stair-stepping or rippling texture on the outside finish [37].

The molds described in the previous section have channels with dimensions on a micro-scale. Some 3D printing devices have low resolution which means that the dimensions in the design may not be correctly reproduced. In order to have a good reproducibility of the designed molds, two different SLA technologies were evaluated, as well as some design guidelines for each one.

SLA was the selected method due to the demanding requirements of the small size features in the molds.

The analysed information is resumed in table 3.1 for the three different SLA technologies, one that uses detail plastic and two others that use frosted ultra detail plastic. The chosen manufacturer was a European company named Shapeways, and the informations summarized in table 3.1 were retrieved from the website of the company (http://www.shapeways.com/materials?li=nav).

Table 3.1: Design guidelines for three different SLA methods.

	Min supported wall thickness	**Min embossed detail**
Detail Plastic	1.0 mm	0.2 mm
Frosted Detail Plastic	0.5 mm	0.2 mm
Frosted Ultra Detail Plastic	0.3 mm	0.1 mm

Figure 3.11 illustrates both guidelines evaluated in table 3.1

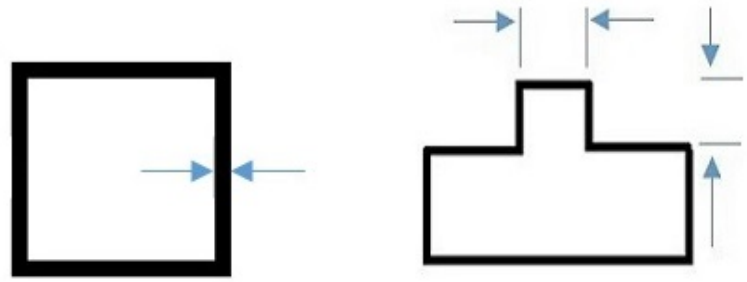

(a) Minimum supported wall. **(b)** Minimum embossed detail.

Figure 3.11: Illustration of both design guidelines evaluated.

A supported wall is a wall connected to others by two or more sides. Its thickness is determined by the ability to successfully clean the printed product once it has been removed from the printer. Walls that are to thin may break when the product is cleaned, which can be prevented when the walls have a thickness bigger than the minimum requirement.

An embossed detail is a feature that sticks out from a surface. The minimum detail is determine by the resolution of the printer. When detail dimensions are bellow the minimum, the printer may not be able to accurately replicate them. In order to avoid that, the details must be larger than the indicated minimum. In this project, for the development of the molds, the most important feature is the minimum embossed detail, since the low height channels fit that type.

3.2.2 Final Molds

The chosen technology, SLA with frosted Ultra Detail Plastic, can achieve the highest resolution and the smallest channel size compare to other available methods. Since the channels are separated by 0.5/0.6 mm, and the walls of the channels have considerable thickness, it was important to ensure that the design was correctly reproduced. With a minimum embossed detail of 0.1 mm, a minimum supported wall of 0.3 mm the micro-scale channels will be surely reproduced.

Since the tactile sensor molds were not as detailed as the strain sensor ones, the chosen material was Detail Plastic, since there was no need for such small minimum embossed detail.

The final printed molds are shown in figures 3.12, 3.13 and 3.14. It should be noted that the mold in 3.14 includes the mold for the pressure sensor and all the flat molds for the layers to isolate the microchannels of the four different sensors.

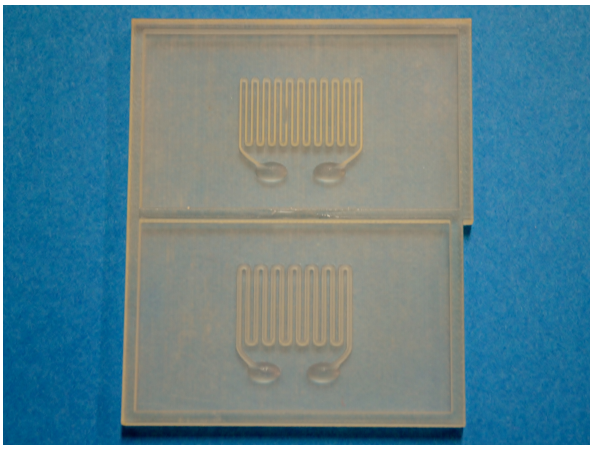

Figure 3.12: Molds for strain sensors printed with SLA Frosted Ultra Detail Plastic technology. The top mold mateches de design shown in figure 3.5, and the bottom mold matches the design shown in figure 3.4.

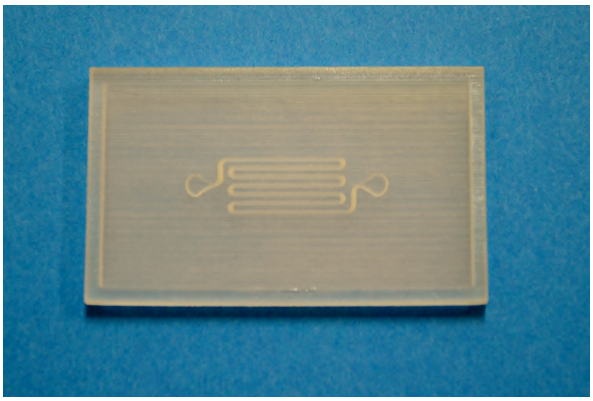

Figure 3.13: Mold for the third strain sensor printed with SLA Frosted Ultra Detail Plastic, matching the design shown in figure 3.6.

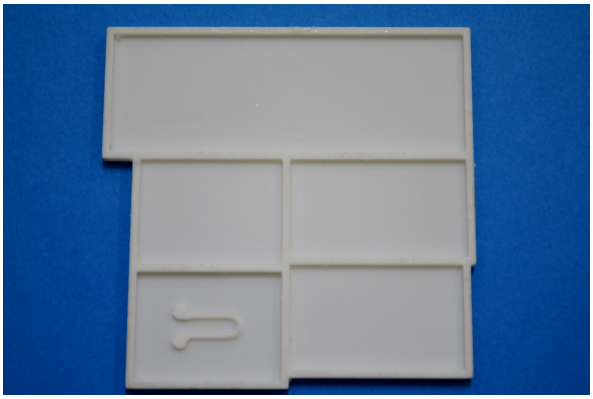

Figure 3.14: Mold for the tactile sensor printed with SLA Detail Plastic Technology, matching the design in figure 3.7.

3.3 Fabrication Process

One of the most important materials of this project is the base substrate of the sensors, which should be a soft and stretchable material. Even though PDMS has good mechanical properties, its polymerization, the reaction that enables the fabrication of polymer chains and three-dimensional networks, is complex if a certain elasticity is required. Thus, similar to [30], [31], [32], [34], the used substrate for this project was Ecoflex®-0030. More specifically, Ecoflex® rubber is a platinum-catalysed silicone, a material that requires that two separate components must be mixed together. One component contains a platinum complex that must be mixed with a siloxane polymer to create an ethyl bridge between the two and originate the silicone rubber.

Working with Ecoflex® requires mixing two components (A and B) in a 1:1 ratio by weight or volume. In their uncured state, Ecoflex® rubbers present low viscosity which ensures easy mixing and de-gasing. In order to turn the viscous liquid rubber into a solid polymer the mixture must cure for several hours at room temperature. When cured, the final product is soft, strong and can stretch almost ten times its rest length without tearing.

Despite having good mechanical properties and being very robust, Ecoflex® also has some drawbacks, including the fact that the curing process can be easily inhibited by low temperature, presence of newly cast or cured polymers in the mixture or in the molds and presence of sulphur components. This turns the fabrication of the membranes into a challenging procedure, since the temperature conditions were not always ideal and the 3D printed molds are not easy to clean due to micro scale features, such as cured silicone from the previous casts.

The major cause of failure in projects dealing with polymers is the lack of knowledge about the nature of the material. Since Ecoflex® is patented and exclusive of a company, there is very little information about its composition, which limited a

deeper chemical structure analysis to investigate its curing and bonding properties. The limitation in available information lead to several attempts to accomplish optimal conditions of the manufacturing process.

In order to find out the optimal conditions for fabrication, several tests were conducted with different parameters. The technical file of the product, available in the Ecoflex-0030 Technical Bulletin in the Appendices at the end of the document, has some important information regarding the processing, mixing, pouring and curing recommendations.

3.3.1 Casting

The first step towards the sensor fabrication is casting, which goes from mixing the two part silicone to pouring it into the 3D printed molds. Before starting, part B was pre-mixed thoroughly for 1 minute. After concluding that pre-mix, the procedure follows the steps illustrated in figure 3.15.

The casting process is the first stage of fabrication. If not done carefully all the other stages will be affected. It is important to ensure that equal parts of silicone are mixed together and that the temperature is adequate to the curing process. Temperatures below 18^o C are known to disable the curing process, and with these conditions, it is necessary to use an oven. If the quality of the membranes is not acceptable, the bonding process will not be well accomplished, and the sensor can most likely suffer from bad isolation of the channels.

Curing of the silicone layers, after exposure to room temperature, at 80^oC for two hours is suggested in the technical bulletin of the material, detailed in Ecoflex-0030 Technical Bulletin in the Appendices. This information was relevant to accelerate the fabrication of the membranes, but had a much more significant role in the bonding process. Therefore, the study of temperature conditions will be further discussed for that stage of fabrication.

1

$15ml$ of Part A and $15ml$ of Part B were homogeneously mixed for at least 3 minutes. Mixing the two silicone components required extreme caution, so that the entrapped air could be minimized.

2

Once the quality of the mixture was acceptable, with little trapped air and with a fine consistency, the liquid rubber was ready to be used. Degassing the mixture is mentioned as optional in the technical bulletin of the silicone.

3

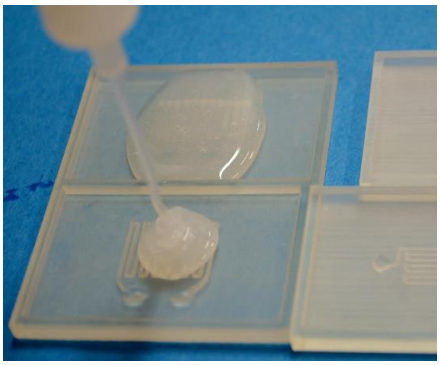

The mixture was poured by a syringe into the molds in a single spot so that the silicone could seek its way up the molds surface. In order to avoid the creation of air bubbles manual spreading was avoided.

4

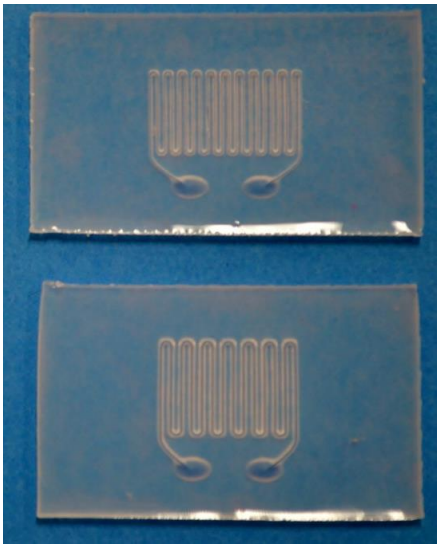

The liquid silicone was left to cure at room temperature for several hours.

Figure 3.15: Ecoflex® Casting steps.

3.3.2 Bonding

After curing at room temperature the membranes were removed from the 3D printed molds and bonded together. This process was challenging due to the Ecoflex® properties. Specifically this kind of silicone rubber is extremely hydrophobic, which means that the silicone has a chemical property that makes it repel water. In fact it really means that this material has low capability of establishing strong links with OH groups, which are most likely present in conventional glues, which makes bonding with other surfaces difficult. Some researchers have come to the conclusion that a thin layer of the same material of the membranes between them is a good solution [9] [30] [34]. This layer has to be thin enough so it does not flow into the microchannels and thick enough so that the membranes will stick together.

3.3.2.1 Post Curing Temperature

Some of the initial attempts to cure the Ecoflex® were unsuccessful, even though the manufacturers guidelines, detailed in Ecoflex-0030 Technical Bulletin in the Appendices, were followed. Some substrates came out of the mold partially uncured, or in a gelly state. Any partial uncured material, even though very small, can compromise the following bonding process. The guidelines were probably good enough for general use of this material, such as in art objects. In the fabrication of the sensors a even cured surface is required. Therefore, several tests were conducted in order to characterize the best curing practice, which was at first important not only to obtain good quality membranes, but also to obtain a layer cured enough so that the blocking of the channels could be prevented.

A simple trial was conducted in which an uncured layer of Ecoflex®, still on its mold, was exposed for 3 minutes at temperatures above 100 ^oC. After that time the silicone was completely cured, even though some air bubbles were trapped in the layer. Acceleration of the curing process seemed to affect the natural de-gasing process of the silicone mixture.

For the bonding process it is important to obtain a layer not fully cured, or in a gelly state. Otherwise, the silicone layer between cured membranes will not establish a stable bond between them.

A second test was conducted, to expose the uncured Ecoflex® for 3 minutes at 60^oC. When the layer was removed from the mold the silicone presented a cured surface, but it was still not fully cured. This trial gave important information about the ideal temperature to cure the thin layer between the two membranes just enough to bond them together. Even though temperature was proven to be important, it was not enough to accomplish good quality layers.

2 ml of Ecoflex® were spread on a flat layer, which was afterwards placed in an oven for 30 s at 60 ^oC to partially cure the material on its surface. After that time the previous layer was placed carefully on top of a layer with engraved microchannels. At the same time, the oven had cool of to 50 ^oC. The assembly of layers was placed in the oven for 15 minutes to accelerate the bonding process. After removing the assembled material from the oven it was perceptible that some Ecoflex® had flown into the channels, which would block the flow of EGaIn during the further injection process. The material between layers was neither thin enough nor well spread. For that reason, the possibility of using the spin coating technique to bond the two layers was considered.

3.3.2.2 Spin-Coating

Similar to [30] [31] [32] the spin coating was the used technique to accurately spread the uncured layer of silicone between the two different layers. This simple method is commonly used to deposit a thin, uniform polymeric film on a flat substrate [38]. A small amount of coating material is usually applied to the center of the substrate, which can be spinning or not at the time of deposition. The user chooses a rotation rate that will influence the thickness of the formed film. The coating material is spread

by centrifugal force. The rotation continues and the excess flows to the edge of the substrate, until the desired thickness of the film is achieved. The thickness of the film depends on the viscosity and concentration of the solution that is deposited on the substrate, as well as on the velocity of rotation of the spin coating plate.

This is a critical step of the fabrication process since the properties of the Ecoflex® film between the layers will influence the quality of the sensor. The technology behind the bonding technique is not complex, though it is hard to get the right conditions so the bonding has an uniform quality that allows sealing of the space between microchannels without entering them.

The first attempt to bring the two layers together was based on the work of a group of researchers from the Harvard University [32]. Their investigation on the subject described that the unpatterned layer should be spin coated at 2000 rpm for 50s although no information was available about the amount of Ecoflex® used in the process. Since there was no previous knowledge on the fabrication of these kinds of sensors, the procedures described in the literature were followed.

Once the spin coater lid was closed, an external vacuum pump was activated, so that the rotational device was safely driven. The desired parameters of the spinning process were entered in the panel, as can be seen in table 3.2. Figure 3.16 shows the used spin-coater, Spin 150.

Table 3.2: Spin coating and partial cure parameters

Amount of Ecoflex® (ml)	**Rotation Speed(rpm)**	**Time (s)**	**Partial cure Temp (^{o}C)**
2,0	2000	50	-

At first the sensors were not subjected to partial cure. A first test was done to evaluate the bonding process at room temperature, with no curing of the layer between the two membranes.

(a) Flat silicone layer placed on the spin-coater, with chosen parameters on the panel.

(b) Spin-coater with the lid closed: the liquid Ecoflex® is poured trough a top hole in the device.

Figure 3.16: Spin-coating device.

When the spin-coater stopped, the layer was carefully removed from the machine and the layer with microchannels was placed on top of it. The assembly was left to cure at room temperature for 1 day. After that time it was clear that the two membranes were not glued, being evident that the layer of the Ecoflex® was not cured. At this point it was possible to conclude that partial cure of the uncured layer in between membranes was necessary. Also to make the bonding easier, placing the assembly in an oven after joining the two layers was considered. There was then a need to perform several tests to find out the right parameters, such as amount of Ecoflex®, parameters of spin coating and the curing time and temperature before and after joining the layers. It should be noted that the key to a successful bonding and sealing of the sensors, is being able to fabricate a uniform layer all over the sensor area.

As it was said, the spin-coater can be already rotating or not when the polymer is poured on the substrate. In order to understand which of the two options would present better results, the sensors were fabricated under both conditions. The chosen

parameters are summarized in the tables 3.3, 3.4.

Table 3.3: Parameters for Spin-coating after pouring Ecoflex®

Sensor	**Amount of Ecoflex® (ml)**	**Rotation Speed(rpm)**	**Time (s)**	**Partial cure Temp (^{o}C)**
Strain 1	1,0	3000	50	50
Strain 2	1,0	2000	50	50
Pressure	1,0	1600	50	50

Table 3.4: Parameters for Spin-coating while pouring Ecoflex®

Sensor	**Amount of Ecoflex® (ml)**	**Rotation Speed(rpm)**	**Time (s)**	**Partial cure Temp (^{o}C)**
Strain 1	1,0	3000	50	50
Strain 2	1,0	2000	50	50
Pressure	1,0	1600	50	50

During the second procedure, the amount of Ecoflex® was measured and poured into the substrate, with syringes whose tube diameter fitted the spin-coater hole that enables the Ecoflex® drop during the rotation of the spin-coater. Since the Ecoflex® is a viscous material, it was extremely difficult to drop it into the layer that was already rotating on the spin-coater.

After a few trials it was clear that 50 s was not enough time to force 1 ml of Ecoflex® out of the syringe. In order to be able to accomplish that, the procedure had to be divided into three steps. The steps were equal, of 40s each, which not only ensures that the whole amount of Ecoflex® is forced out of the syringe, but also makes the uncured layer of Ecoflex® thicker and more uniform, since it suffered the action of spin-coating three times.

The sensors fabricated under the conditions summarized in Table 3.3 all failed to be sealed. At the sime time, acceptable results were obtained in the trials resumed in Table 3.4. The strain sensors 1 and 2 presented a cured layer on the flat membrane but there was no link between that membrane and the one with the microchannels. Since the rotation speed for those two sensors was 3000 and 2000 *rpm* respectively, this probably means that the layers were to thin. The pressure sensor, for which the flat layer was rotated at 1600 *rpm* was well sealed. Following the parameters chosen for the pressure sensor a final fabrication procedure could be established.

3.3.2.3 Final Fabrication Procedure

Even though the dimensions of the sensors were not equal, the same amount of Ecoflex® was used, since the differences can be unvalued.

- The cured layers are removed from the molds.
- The flat layer is placed in a piece of glass which is then placed on a spin-coater.
- As the device starts to rotate, Ecoflex® is pushed of a syringe to the rotating layer for 40s. This process needs to be divided since the Ecoflex® is extremely viscous and is more effectively spread if the process is repeated more than once .
- When the spin-coater is stopped, the lid is opened and the layer with the uncured Ecoflex® is placed in an oven at 50^{o}C for 30s.
- The layer with the channels covers the flat layer and the assembly is placed in the oven, at 50^{o}C for 15 minutes.

3.4 Eutectic Gallium-Indium (EGaIn)

In this section the behaviour and properties of the liquid metal eutectic gallium-indium (EGaIn) are described. EGaIn is a liquid metal alloy with 75% Gallium and 25% Indium by weight with appealing properties for applications in electronics [39] The fact that it remains in a liquid state at room temperature makes it a fitted solution to rapidly fill channels when submitted to sufficient pressure. This ability is important since it enables the formulation of low cost systems for stretchable electronics that can go from microscale wires to circuit elements or electrodes.

Figure 3.17 shows a closer look to this metal and its ability to easily adhere to surfaces.

Figure 3.17: EGaIn drop: From left to right: The metal alloy suspended from a needle, brought into contact with a surface. At some point the material adheres to both of them. [39].

EGaIn is a metal alloy commercially available. For the present application it is preferable to Mercury (Hg) due to its non-toxic properties, and is easier to inject than other materials that, as mentioned before, are time consuming. EGaIn has certain attributes that sustain the choice made to use this material:

1. EGaIn is electrically conductive. It has a resistivity of $29,4 \times 10^{-6}\ \Omega m^{-1}$.

2. This alloy has the ability to shape into a stable free-standing structure, which makes it extremely moldable.

3. It has low viscosity $1,99 \times 10^{-3}$ Pa.s, a property that allows it to flow readily, be easily injected, and be used as an electrically conductor.

4. Its components have low orders of toxicity. This makes it superior to Hg that is a good solution for injection in microchannels but is extremely toxic.

5. At room temperature it makes conformable, non damaging contact with surfaces.

3.4.1 Injection

The material tends to adopt a spherical shape when it is not confined to a recipient or a channel, which is the case in this project. For this reason the liquid metal was injected with the help of two syringes in a single movement. This step needs to be done carefully, since too much pressure or bad placement of the syringe can puncture or even totaly rupture the silicone material. Figure 3.18 shows an example of a bad injection process.

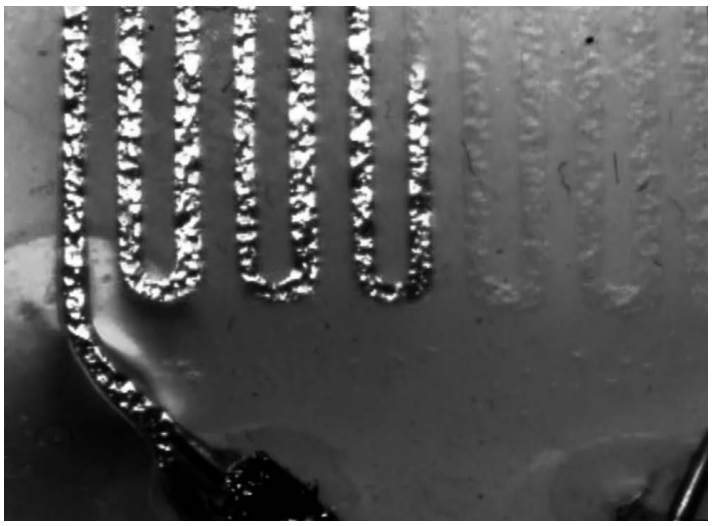

Figure 3.18: Injection of the EGaIn in the microchannels, captured with a Leica Microscope. In the left bottom corner of the caption it is visible that the sensor was ruptured, which resulted in an undesired flow of EGaIn throughout the channels.

The right way to inject this material is with the help of two syringes of 1ml capacity. One of the syringes injects the material and the other pulls the air out of the channels, which needs to be evacuated to enable the normal flow of EGaIn inside the microchannels.

The syringes were inserted in the injection points identified with the number 3 in figures 3.4a, 3.5a, 3.6a and with the number 1 in figure 3.7a. Since the channels have a thickness of 1 mm, this procedure needs to be done carefully so that the material is not perforated, which can cause the rupture of the channels and the escape of the metal from them.

To complete the fabrication of the sensor it is crucial to isolate the injection points. This is accomplished by pouring liquid Ecoflex® in the injection area after inserting electrical wires that are necessary for the characterization process described in the next chapter. This isolation ensures that the metal does not come out of the sensor.

3.5 Lessons Learned

The fabricated sensors can only have a good performance if the fabrication process is followed and completed correctly. Even though the materials are easy to manipulate and the presented technology is quite simple to fabricate, the limitations of some equipments made the fabrication of the sensors more difficult than expected.

There are some bad experiments that are briefly reported so that further work can be easier and not delayed or compromised by mistakes in fabrication. With this small report further work in this research area can be simplified.

Illustrations of failed tests are presented and the reasons for their occurrence are reported.

As mentioned in Chapter 3 the Bonding step is crucial to ensure that the microchannels can be correctly injected with conductive liquid metal. If the layers are not well bonded together the microchannels will have areas where the connection between adjacent channels is not well established. This problem is shown in figure 3.19.

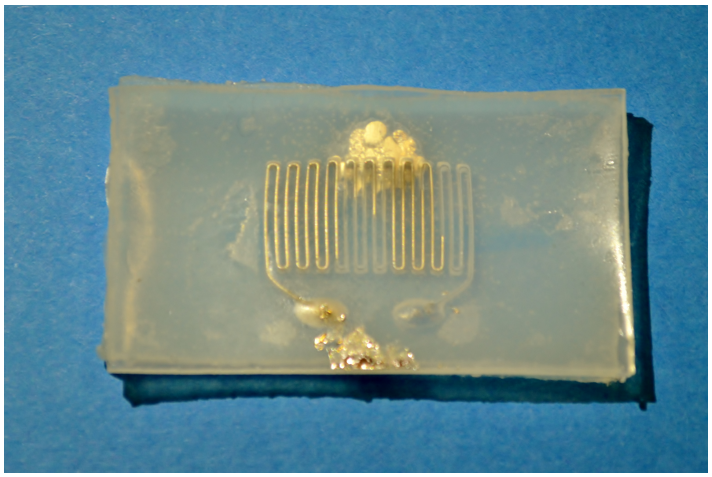

Figure 3.19: Example of failed bonding process.

Bad isolation, or more specifically, bad assembly of the two membranes of Ecoflex®, is caused mostly by the amount of liquid silicone spread in the flat surface that will act as glue between the two layers. The rotation speed in the spin-coating process is also important since it influences the thickness of the layer which has to be significant to glue the two parts but thin enough so that the microchannels are not filled with the material. In some cases the two layers seemed to be well bonded, but during the injection process it was visible that, even though the microcahnnels were not blocked, the area around them was not well sealed. In that case the liquid metal escaped from the channels and spread through the free area around them. Figure 3.20 shows a prototype which illustrates the problem previously reported.

Though it was simple to inject the sensors with EGaIn it was tricky to ensure that the channels were completely filled with the liquid metal. Sometimes during the extraction of the captured air with the second syringe some of the injected metal flowed inside it, which meant that the metal inside the sensor was injected in excess. Nevertheless if the injection points are not sealed, the metal continues to come off the sensor which can

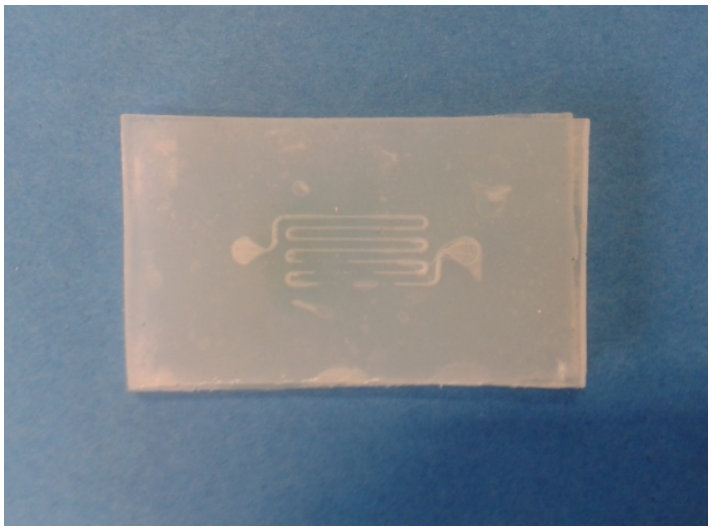

Figure 3.20: Example of blocked microchannels.

cause a deflation of the channels, compromising their electrical functionality. Figure 3.21 shows a fabricated prototype whose injection points were not sealed with Ecoflex® material. Liquid metal is visible outside the microchannels, which due to its properties tends to adopt a spherical form.

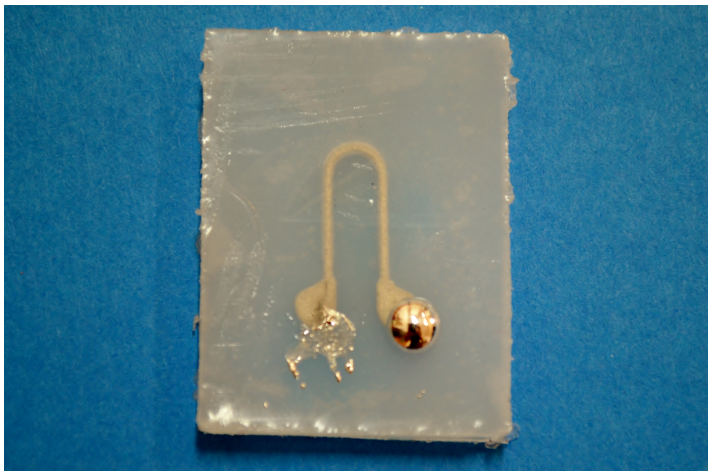

Figure 3.21: Example of metal coming off the sensor.

The reported problems can be avoided, which requires multiple sensors fabrication in order to expertise the process. That was one of the most important goals of this project, expertise and understand the process of fabrication of stretchable sensors that can have good quality, good performance and are fabricated with relatively low cost methods.

Since this technology is recent and extremely useful and with a wide range of applications it is important to study and report the fabrication of such devices.

Since this is a growing technological field it is expected that the work developed in this final project can contribute to simpler fabrication of further stretchable devices using similar materials and techniques.

Chapter 4

Results and Discussion

In this chapter the final fabricated sensors and the characterization of the devices are presented. The practical implementation of the calibration procedures and the results are also discussed according to expected theoretical data.

4.1 Sensors Characterization

Four different prototypes were fabricated, as shown in figure 4.1.

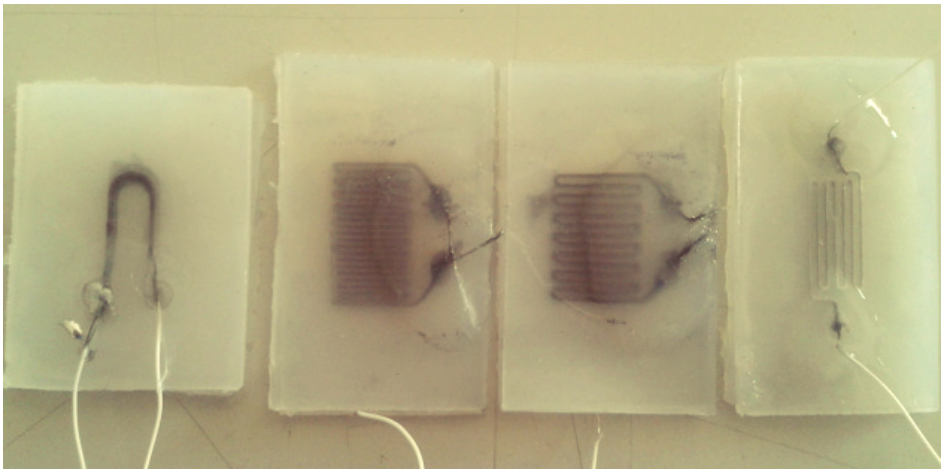

Figure 4.1: Final fabricated sensors. From left to right: Pressure sensor; Strain sensors: 400 μm, 800 μm and 600 μm respectively.

A first trial was conducted to understand the behaviour of the silicone rubber, used in the fabrication of the sensors, when submitted to significant elongations. After testing the silicone material, the four different devices were tested with simple methods to understand their response to two different stimulus, strain and pressure.

The practical implementation of the characterization procedure and the resulting models established from that study are as well presented and discussed.

4.1.1 Methodology

The study of the used elastomer was conducted by fixing a fabricated prototype, with no liquid metal in the microchannels, in an universal testing machine. The sensor was fixed by two gripers, one that remained static and other movable that was extending the silicone material. The material was gradually stretched with a rate of 10 mm/s up to three times its rest length, in the x-axis. The results from this pilot study are shown in figure 4.2.

The behaviour of the material is quite similar to the predicted theory presented on Chapter 2 and visible in figure 2.4. The material has a linear response to the applied stress and can sustain large elongations. It has a good behaviour which indicates that it will most likely not rupture during the strain trials. This was important to ensure that the sensor did not rupture easily which could be a problem since the liquid metal is extremely hard to clean from surfaces.

After testing the material, the change in electrical resistance ΔR of the embedded EGaIn channels was measured as a function of the applied strain and pressure using the two different experimental setups shown in figures 4.3 and 4.4.

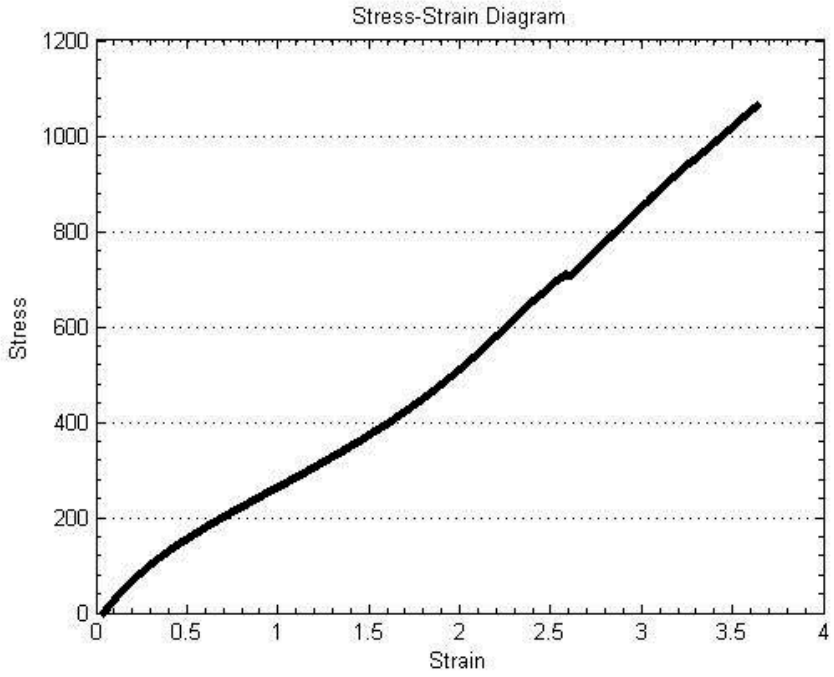

Figure 4.2: Strain-Stress diagram for a tested membrane of cured Ecoflex®.

The pressure sensor prototype was characterized by compressing the center of the sensor up to 15 kPa. A rigid surface with an area A=0,0004 m^2 is pressed into the sensor with a Center Drive 5" Square Linear Translation Stages shown in figure 4.3b. The device has a movable part that was adjusted to gradually compress the sensor. The sensor was supported by a digital scale (12 Kg) that measured the force F exerted on the surface of the sensor. The pressure exerted over the area of contact was calculated according to 4.1.

$$p = \frac{F}{A}, \tag{4.1}$$

with F the applied force, and A the area of the surface pressed into the sensor. The ends of the microchannels were wired to a precision multimeter (Hewlett Packard 34401A with a $6^{1/2}$ digits resolution) that measured the change in electrical resistance.

(a) Digital multimeter Hewlett Packard 34401A, using the 4-wire ohms method to measure the resistance.

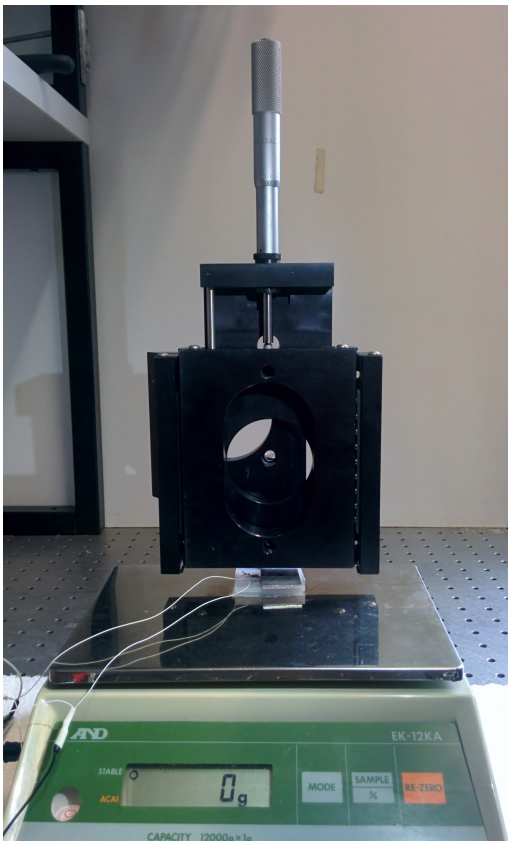

(b) Digital scale with 12 kg capacity measuring the force applied by the height gauge.

Figure 4.3: Experimental setup for simultaneous measurements of applied pressure and electric resistance for the fabricated pressure sensor.

The strain prototypes were characterized by applying strain in the x-axis direction using an universal material tester (Shimadzu AG-X). The sensors were stretched up to 100%. The rest length of the sensors was 23 mm, and with the help of two tweezers, visible in figure 4.4b, they were fixed in the testing machine by two gripers, one that remained static and another movable that was extending the devices. They were gradually and manually stretched so it was possible to register the displacement values and the resistance change simultaneously. The ends of the microchannels of the sensors were again wired to a digital multimeter that measured the change in electrical resistance.

(a) Digital multimeter HP 34401A, using the 4-wire ohms method.

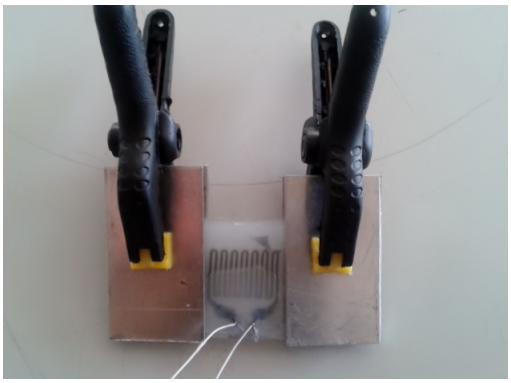

(b) Sensor fixed by two tweezers separated by a fixed distance of 23 mm.

(c) Strain sensor in an universal testing Shimadzu AG-X to perform the x-axis strain test

Figure 4.4: Experimental setup for simultaneous measurements of x-axis strain and electric resistance for the fabricated strain sensors.

An initial trial to test the working concept of the designed devices, showed that the nominal resistance of the sensors was low. The Hewlett Packard 34401A digital multimeter offers two methods to low resistance measurements: 2-wire and 4-wire ohms. For both methods the current flows from the input terminal and then through the resistance that is being measured. The 4-wire method provides a more accurate way to measure small resistances [40] [41].

The main problem with the two-wire method, when applied to low resistance measurements, is that the total lead resistance is added to the measurement. Since the test current causes small but significant voltage drop across the lead resistances, the voltage measured by the multimeter will not be exactly the same as the voltage directly across the resistance, and errors can result from this method.

With the four-wire configuration, the test current is forced through the test resistance through one set of leads, while the voltage is measured through a second set of leads called sense leads. The current that flows through the sense leads is negligible, so the voltage measured by the multimeter is essentially the same as the voltage across the resistance.

The connections for 4-wire ohms measurements are shown in figure 4.5.

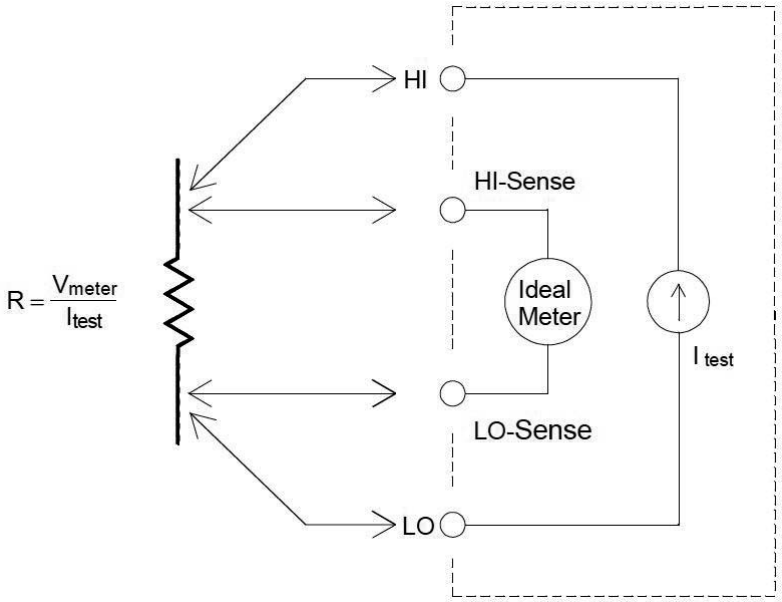

Figure 4.5: Four-Wire Resistance Measurement [41].

4.1.2 Results and Discussion

The mechanics of the embedded microchannels in the designed strain sensor is complex and can be modelled only by an approximate mathematical analysis.

The resistance of a conductive elastomer can be calculated using the resistivity of the conductive material and the physical dimensions of the elastomer [42]:

$$R = \frac{\rho L}{A}, \tag{4.2}$$

where ρ is the electric resistivity of the conductive material while L and A are the length and the cross-section area of the microchannel respectively. Using the relation given by 4.2 the change in resistance:

$$\Delta R = (R + \Delta R) - R, \tag{4.3}$$

can be expressed by the equation 4.4.

$$\Delta R = \rho \frac{L + \Delta L}{A + \Delta A} - \rho \frac{L}{A} \tag{4.4}$$

Since the cross section area is given by the product between the width w and the thickness h, equation 4.4 can be rearranged to:

$$\Delta R = \rho \frac{L + \Delta L}{(w + \Delta w)(h + \Delta h)} - \rho \frac{L}{wh} \tag{4.5}$$

If a rod with a certain width and thickness is subjected to tension, its length will change as well as the width and thickness according to the following relations:

$$\Delta w = -w\nu\varepsilon \tag{4.6}$$

$$\Delta h = -h\nu\varepsilon, \tag{4.7}$$

where ν is the Poisson's ratio of the material. Replacing these relations in 4.5 and since ε=ΔL/L,

$$\Delta R = \frac{\rho L}{wh}\left(\frac{(1+2\nu)\,\varepsilon - \nu^2\varepsilon^2}{(1-\nu\varepsilon)^2}\right) \tag{4.8}$$

Since in this project the base material of the sensors is an elastomer, the Poisson's ratio is ν=0.5, which can be used to simplify the previous equation:

$$\Delta R = \frac{\rho\varepsilon L(8-\varepsilon)}{wh(2-\varepsilon)^2} \tag{4.9}$$

The obtained equation establishes a relation between the change in resistance and the applied deformation. With this information it was possible to compare the experimental data to the one expected according to the mathematical deduced model. The results from all the calibration procedures are detailed in the Experimental Data Appendix at the end of this document.

In the first calibration trial the microchannels of the device had a width w=0.8 mm, a height h=1 mm, a rest length L=12,5 mm and an electric resistivity ρ=29,4 $\times 10^{-8}$. Fitting the equation 4.9 to the experimental data using the method of least squares, it was possible to compare the obtained results with the theoretical ones.

For a single channel the constants ρ, L, w and h are known, and so it was possible to obtain the theoretical relation for the change in electrical resistance as function of the applied strain. Figure 4.6 shows only an example of the theoretical predicted behaviour for one single channel of the strain device with microchannels of 800 μm width. There is no significant differences in the theoretical predictions, for a single channel, between the three fabricated strain sensors.

The experimental results of this trial, as well as the theoretical results are shown in 4.7. The data collected in this trial is organized in tables 1 and 2, in the Experimental Data appendix at the end of this document.

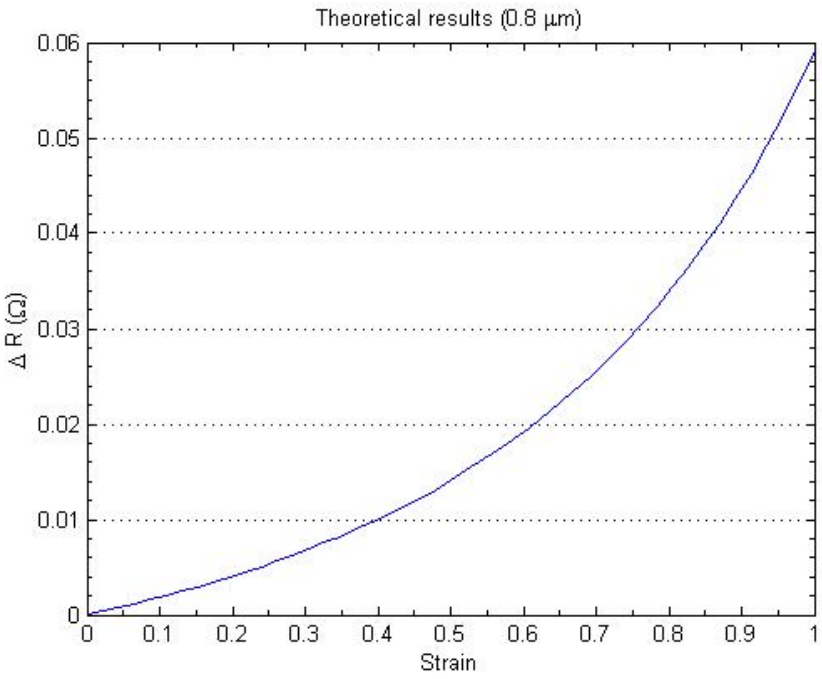

Figure 4.6: Theoretical results for the change in electrical resistance as function of the applied strain, for a single channel of width w=800 μm.

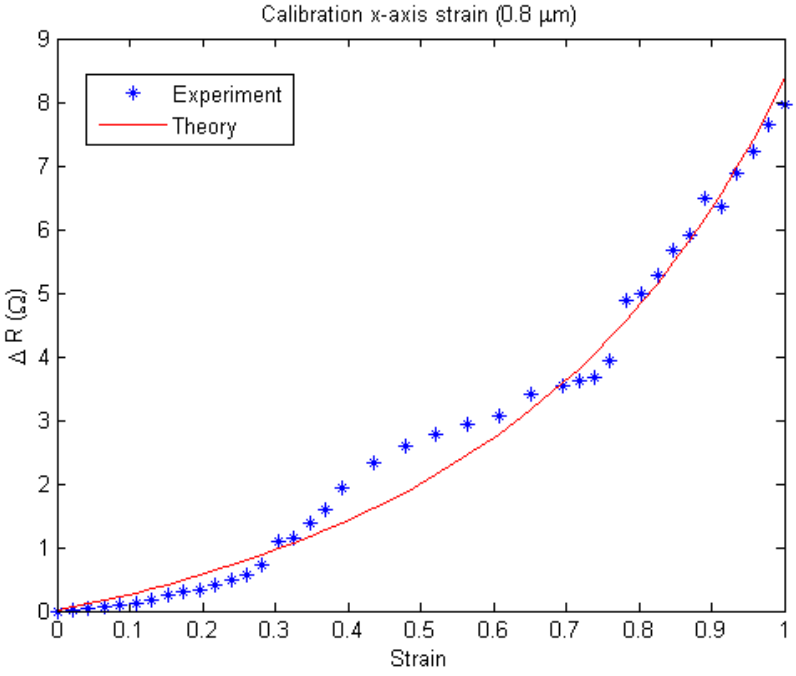

Figure 4.7: X-axis strain characterization for the strain sensor with microchannels with 800 μm width.

By comparing the theoretical and the experimental results it is clear that the behaviour of the sensor is in agreement with the mathematical function deduced previously. In terms of repeatability it was not possible to obtain relevant results. When stretched repeatedly the sensor showed some failure in the wire connection site. After two trials and excessive stretching the wires were disconnected from the channels. Rewiring the ends of the microchannels could cause changes in the nominal electric resistance of the sensors and the repeatability will not be correctly evaluated.

If the behaviour of the devices was approximately linear, it would be possible to obtain a linear fitting of the extracted data. The linear function would enable the calculation of the gauge factor, which can be defined as a measure of the sensitivity of the strain sensor or its resistance change per unit applied strain, and is given by 4.10 [42].

$$\frac{\Delta R}{R} = G\varepsilon, \tag{4.10}$$

assuming that the temperature change is negligible.

Since there is a non-linear behaviour this factor, commonly known in conventional strain gauges, could not be calculated with the previously presented equation.

The second calibrated sensor had a width w=0.4 mm, a height h=1 mm, a rest length L=12,5 mm and an electric conductivity ρ=29,4 $\times 10^{-8}$. The experimental and theoretical results for the change in electrical resistance as function of the applied strain are shown in figure 4.8. The results of this trial are organized in table 3 in the Experimental Data appendix at the end of this document.

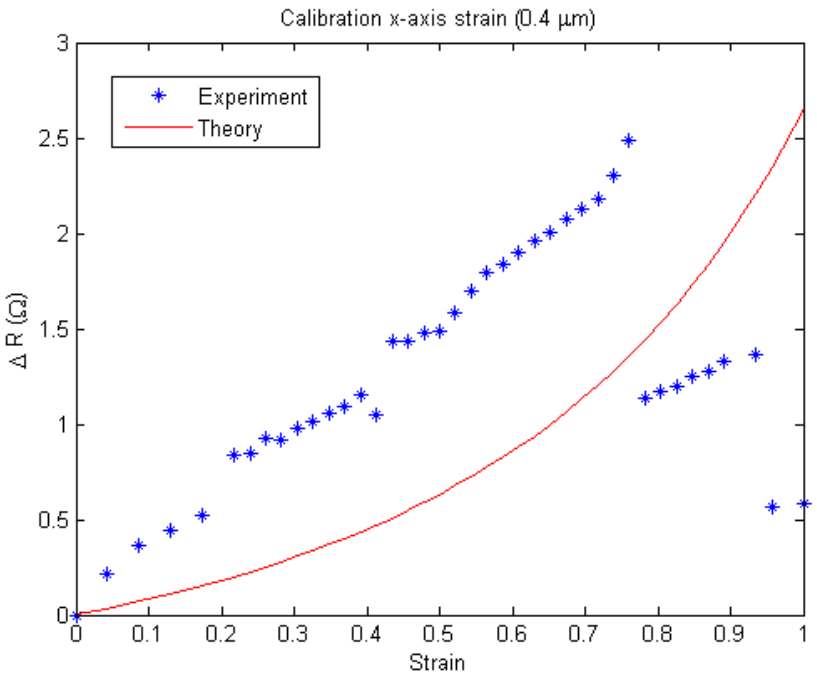

Figure 4.8: X-axis strain characterization for the strain sensor with microchannels with 400 μm width.

The second tested strain sensor showed an unexpected behaviour. The change in electrical resistance as function of the applied strain did not follow the theoretical predictions. When the deformation reached 0.7 the change in electrical resistance started to decrease, which was not expected. At first this seems to be a signal of rupture of the substrate material, but after taking the device of the used machine neither rupture nor serious deformations were found.

The last of the strain sensors to be characterized was the sensor with width w=0.6 mm, height h=1 mm, rest length L=14 mm and an electric conductivity ρ=29,4 $\times 10^{-8}$. The experimental and theoretical results, showing the change in electrical resistance as function of the applied strain are shown in figure 4.9. The experimental results are organized in table 4, in the Experimental Data appendix at the end of this document.

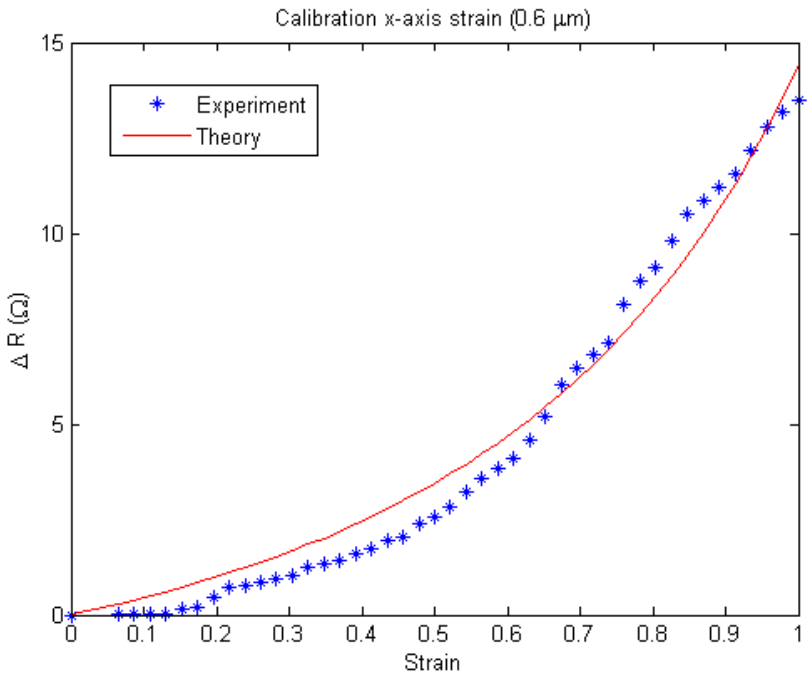

Figure 4.9: X-axis strain characterization for the strain sensor with microchannels with 600 μm width.

The strain response of the third sensor is the one that shows the best accordance to the theoretical expectations. It should be noted at this point that the sensors were strictly subjected to strains in the X-axis direction. When a material experiences strain in the axial direction of its channels, the overall channel length increases and the cross-sectional area decreases. For the two first calibrated sensors the strain was applied to the X-axis direction while the channels of the sensors were oriented along the Y-axis. Thus, it is expected that the response of the third sensor has a closer behaviour to the theoretical predictions.

The last sensor to be characterized was the pressure sensor. Three tests were performed so that the repeatability could be evaluated. The microchannels of the calibrated pressure sensor had a width w=0.8 mm, a height h=1,5 mm, a rest length L=12,5 mm and an electric conductivity ρ=29,4 $\times 10^{-8}$. With the previous constants, according to Linear Elastic Fracture Mechanics (LEFM) [43] and the work developed by Park et al [30] the theoretical results for the change in electrical resistance ΔR as a function of the applied pressure were determined following the equation 4.11.

$$\Delta R = \frac{\rho L}{wh}\left\{\frac{1}{1-2\left(1-\nu^2\right)wp/Eh}-1\right\}, \tag{4.11}$$

where ρ is the electric resistivity of the conductive material and L, w and h the length, width and height of the channels, respectively. p is the applied pressure while ν and E are the Poisson's ratio and the Elastic modulus of the elastomeric material.

Applying this function to the experimental results for the applied pressure, theoretical values of change in resistance were obtained. The predicted results, for a single channel, are shown in figure 4.10 while the experimental results are shown in 4.11.

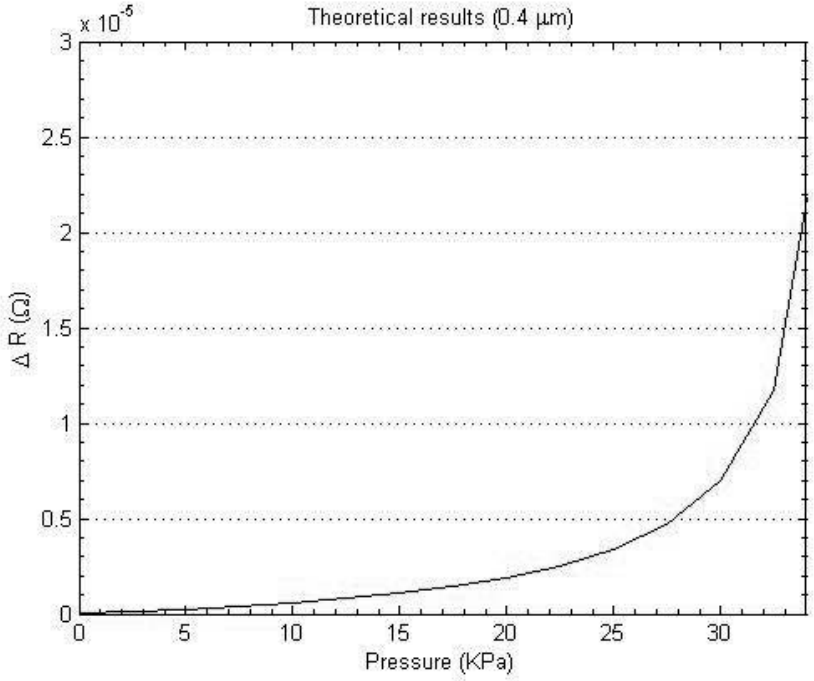

Figure 4.10: Theoretical relationship between resistance change (ΔR) and the applied pressure (KPa).

The pressure response was studied by applying compression three times at the center of the top surface with a flat surface with width w=20mm and length L=20mm. Figure 4.11 shows that the change in the electrical resistance as function of the applied pressure occurs as expected.

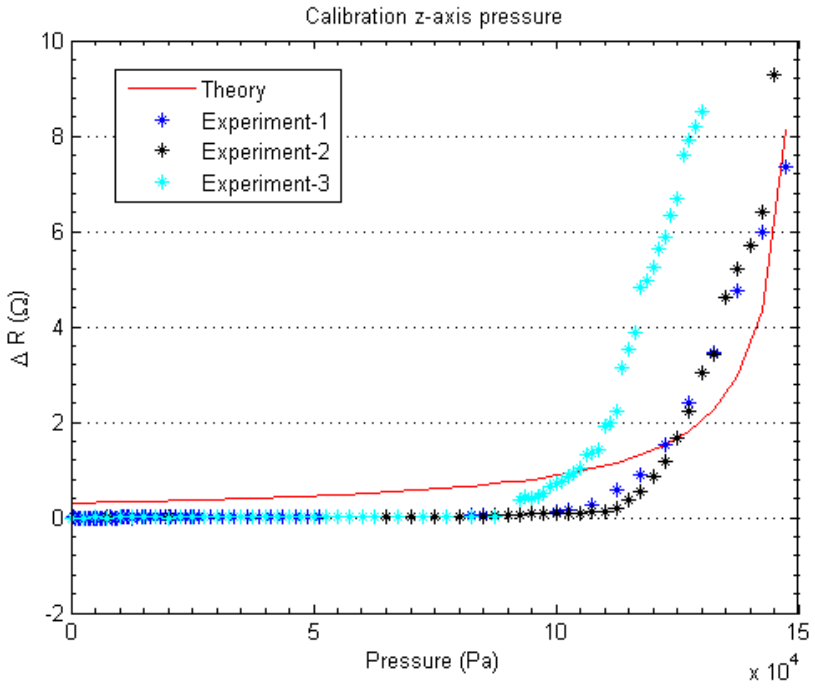

Figure 4.11: Z-axis characterization for the pressure sensor with microchannels with 800 μm width.

When pressed, the elastomer suffers deformation, the cross-sectional area of the microchannels decreases, which increases the electrical resistance, according to the expression 4.11. The pressure response is non linear, again as it was predicted after analysing the theoretical information. The minimum average detectable pressure is $11KPa$, and the sensor showed repeatability, since the three trials showed similar results.

For the sensors with the design illustrated in figures 3.4, 3.6 and 3.7, the experimental results are in accordance with the theory for a wide range of applied pressure and strain. Some observed discrepancies are due to the simplified assumptions, in the theoretical models, that the channels have square cross-sectional areas, which is not the case.

The purpose of a sensor is to respond to an input physical property and to convert it into and electrical signal that is compatible with electronic circuits. Usually the output of a sensor is in the form of voltage, current or charge. In this particular case the measured output is the electrical resistance. By knowing the behaviour of the sensors, and measuring the sensors output it is possible to obtain information about the applied strain or pressure. These informations are valuable and can have multiple applications, like the measurement of the bending angle of a human/robotic finger or the contact pressure between robotic fingers and an object [26], [33].

As it was already mentioned at the end of Chapter 3, injecting the liquid metal into the channels is simple while ensuring that the microchannels are completely filled is sometimes difficult. As consequence of poor injection, the metal gets free space to flow along the channels, and so the changes in electrical resistance can be compromised. The results from the strain sensor with 400 μm microchannels can be explained by this problem, since after two trials it was clear that some free spaces in the channels have started to appear.

Another major problem found during the characterization trials was the wire connections. The choice of the used wires did not followed a rigorous criteria, they were used since their diameter was small and could fit the injections points without causing any damage to the fabricated prototypes. The situation where the wire connections were counter productive was in the characterization of the strain sensors. The repeatability could not be evaluated due to failure in the connection points after subjecting the devices to significant deformation.

As it was mentioned before a sensor is sensitive to deformation in the axial direction of its designed channels. The two first sensors showed good responses to deformation, in spite of the non-expected behaviour of the second one. This can be explained by the curve links between channels, that are oriented in the direction of the applied strain during the characterization trials.

The devices show a good overall behaviour, and their responses in terms of resistance are reliable. Nevertheless the absolute difference between the nominal resistance and the resistance when pressed or stretched is quite small. Low resistivity also makes the sensors sensitive to electrical noise and variations due to movement of connecting wires.

Chapter 5

Conclusion

5.1 General Conclusions

The work developed in this project managed to study the fabrication methods and materials to develop soft resistive sensors for strain and pressure sensing. In fact four different working prototypes were developed that can contribute to understand a few more aspects about the field of tactile sensors and stretchable electronics.

The main goal of this project was to study and expertise the fabrication of strain and pressure sensors. The fact that the fabrication process of the sensors was not well established led to unexpected problems and delays in the development of the prototypes. Even though valuable lessons were learned that can be considered in the future to obtain more effective and quick results.

The devices were built and tested showing overall acceptable performance and a behaviour that can be modelled by mathematical approximations. For the pressure sensor the results were in average in accordance with the theoretical predictions, and pressures up to 15 KPa were detected with no report of saturation of the sensor. The sensor also showed good repeatability.

The three sensors designed for strain sensing showed different behaviours between them. The first two designed sensors had microchannels oriented in the y-axis direction while the applied deformation was along the x-axis. For that reason it was expected that the third designed sensor, with microchannels oriented in the axial direction of deformation showed better responses to strain with bigger variations of electrical resistance. The sensors showed a good performance for deformations up to 100% their rest length. The repeatability was not evaluated due to failure in the wire connections during most of the characterization tests.

Although the devices showed good working performance they are far from providing sufficient information about multiple stimulus. This is a crucial requirement in robotics, especially in projects that aim to develop assistive devices. The technology studied in this project has the potential to aid future advancements in areas such soft electronics and wearable robotics.

An increase in the demand and update of tactile sensing technologies has been observed in the last few years. This indicates that there is always a need for future work and that all contributions are important to understand the basics and move from that to much complex and complete technologies. With its clear limitations this work contributed with good multidisciplinary knowledge base to future exciting developments in the artificial tactile sensing area.

The field of Biomedical Engineering combines engineering with medical and biological sciences to advance healthcare treatments. The application of the developed work to prostheses, even though further improvements have to be done, can contribute to improve the quality of prosthetic devices. More importantly it can improve the life quality of amputees, since the manipulation of objects can now be followed by feedback, which is extremely important for a wide range of tasks performed in daily activities.

5.2 Future Work

The presented work is an important aspect in a project that intends to create a prosthetic hand capable of restitution sensing capabilities to amputees. Even though it was not possible to integrate the developed sensors on a robotic finger, that option was studied and an example is shown in figure 5.1. This is a simple integration example of the pressure sensor, by using uncured Ecoflex® between the coloured polymer in the finger and the silicone substrate of the sensor. A detailed study is needed for good and reliable integration of the fabricated soft sensors in the fingers of the ISR Softhand.

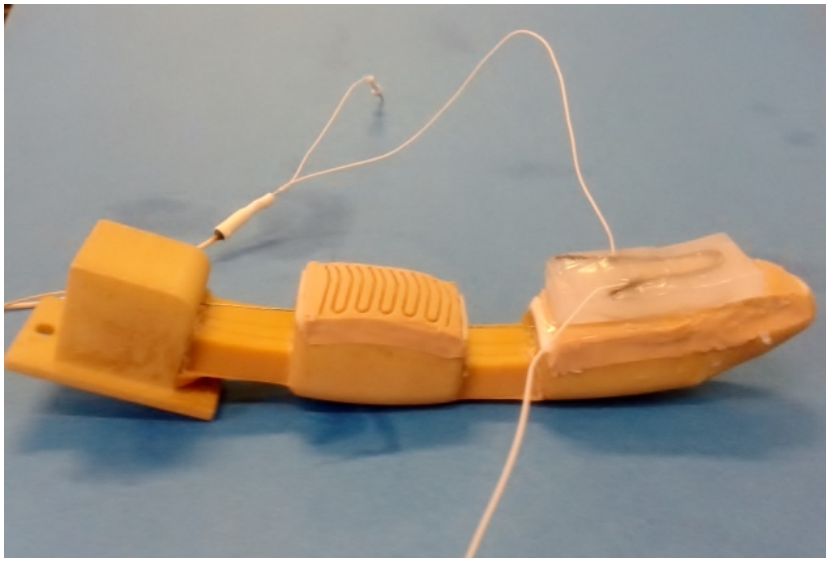

Figure 5.1: Example of possible integration o the pressure sensor.

Although the smallest channel size is 400 μm, these dimensions could be further reduced since it was proven by this work that is possible to properly seal such small structures for posterior injection of liquid metal. 3D printing technologies have some limitations, and as far as having features smaller than 200 μm the best solution is to study other manufacturing methods, like micromachining. This method builds microstructures by deposition and etching of different structural layers on top of a substrate. The application of this method to soft substrates is an interesting option to design microchannels with smaller dimensions than the ones presented by this project.

Another main challenge of this work was routing the strain and pressure signals, which can be improved by studying and testing softer wires that can follow the deformation of the sensors and not compromise the experimental results. EGaIn was the chosen conductive liquid due to its appealing properties such as good resistivity and conformable behaviour at room temperature. Nevertheless if the sensors are subjected to a random deformation it can be understood as strain or pressure even when that is not the case. Ionic solutions are a good alternative for the sensing part of the sensors while the conductive metal can be only used for routing the electric signals to adequate electronics. This was already studied by Park et al. [44], and can be considered in future developments of this kind of technology.

Complete artificial skins that show multiple sensing capabilities should also be considered. Future work on an artificial skin glove that can fully cover a robotic prosthetic hand, will focus in arrayed structures, once the basic principles of soft electronics are well established.

Bibliography

[1] R. R. Ma, L. U. Odhner, and A. M. Dollar, "A modular, open-source 3d printed underactuated hand," in *Robotics and Automation (ICRA), 2013 IEEE International Conference on.* IEEE, 2013, pp. 2737–2743.

[2] S. Patel, H. Park, P. Bonato, L. Chan, and M. Rodgers, "A review of wearable sensors and systems with application in rehabilitation," *Journal of neuroengineering and rehabilitation*, vol. 9, no. 1, p. 21, 2012.

[3] Y.-L. Park, B.-r. Chen, C. Majidi, R. J. Wood, R. Nagpal, and E. Goldfield, "Active modular elastomer sleeve for soft wearable assistance robots," in *Intelligent Robots and Systems (IROS), 2012 IEEE/RSJ International Conference on.* IEEE, 2012, pp. 1595–1602.

[4] W. K. Purves, G. H. Orians, D. Sadava, and H. C. Heller, *Life: The Science of Biology.* Sinauer Associates, Inc, 2011, vol. 9.

[5] M. I. Tiwana, S. J. Redmond, and N. H. Lovell, "A review of tactile sensing technologies with applications in biomedical engineering," *Sensors and Actuators A: physical*, vol. 179, pp. 17–31, 2012.

[6] E. Pfeiffer, C. Rhode, and S. Fabric, "An experimental device to provide substitute tactile sensation from the anaesthetic hand," *Medical and biological engineering*, vol. 7, no. 2, pp. 191–199, 1969.

[7] J. M. Romano, K. Hsiao, G. Niemeyer, S. Chitta, and K. J. Kuchenbecker, "Human-inspired robotic grasp control with tactile sensing," *Robotics, IEEE Transactions on*, vol. 27, no. 6, pp. 1067–1079, 2011.

[8] Y.-L. Park, B.-r. Chen, D. Young, L. Stirling, R. J. Wood, E. Goldfield, and R. Nagpal, "Bio-inspired active soft orthotic device for ankle foot pathologies," in *Intelligent Robots and Systems (IROS), 2011 IEEE/RSJ International Conference on.* IEEE, 2011, pp. 4488–4495.

[9] Y. Menguc, Y.-L. Park, E. Martinez-Villalpando, P. Aubin, M. Zisook, L. Stirling, R. J. Wood, and C. J. Walsh, "Soft wearable motion sensing suit for lower limb biomechanics measurements," pp. 5309–5316, 2013.

[10] Y.-L. Park, J. Santos, K. G. Galloway, E. C. Goldfield, and R. J. Wood, "A soft wearable robotic device for active knee motions using flat pneumatic artificial muscles."

[11] T. Sagisaka, Y. Ohmura, Y. Kuniyoshi, A. Nagakubo, and K. Ozaki, "High-density conformable tactile sensing glove," in *Humanoid Robots (Humanoids), 2011 11th IEEE-RAS International Conference on.* IEEE, 2011, pp. 537–542.

[12] A. Drimus, G. Kootstra, A. Bilberg, and D. Kragic, "Design of a flexible tactile sensor for classification of rigid and deformable objects," *Robotics and Autonomous Systems*, vol. 62, no. 1, pp. 3–15, 2014.

[13] R. S. Dahiya, G. Metta, M. Valle, and G. Sandini, "Tactile sensing—from humans to humanoids," *Robotics, IEEE Transactions on*, vol. 26, no. 1, pp. 1–20, 2010.

[14] M. S. C. Tee, Benjamin C.K. and Z. Bao, *Elastomer - Based Pressure and Strain Sensors*, 1st ed. John Wiley & Sons, 2012.

[15] H. Yousef, M. Boukallel, and K. Althoefer, "Tactile sensing for dexterous in-hand manipulation in robotics—a review," *Sensors and Actuators A: physical*, vol. 167,

no. 2, pp. 171–187, 2011.

[16] P. S. Girão, P. M. P. Ramos, O. Postolache, and J. Miguel Dias Pereira, "Tactile sensors for robotic applications," *Measurement*, vol. 46, no. 3, pp. 1257–1271, 2013.

[17] C.-H. Chuang, W.-B. Dong, and W.-B. Lo, "Flexible piezoelectric tactile sensor with structural electrodes array for shape recognition system," in *Sensing Technology, 2008. ICST 2008. 3rd International Conference on.* IEEE, 2008, pp. 504–507.

[18] P. Puangmali, K. Althoefer, L. D. Seneviratne, D. Murphy, and P. Dasgupta, "State-of-the-art in force and tactile sensing for minimally invasive surgery," *Sensors Journal, IEEE*, vol. 8, no. 4, pp. 371–381, 2008.

[19] R. D. Ponce Wong, J. D. Posner, and V. J. Santos, "Flexible microfluidic normal force sensor skin for tactile feedback," *Sensors and Actuators A: Physical*, vol. 179, pp. 62–69, 2012.

[20] V. Ho, M. Makikawa, and S. Hirai, "Flexible fabric sensor toward a humanoid robotic skin: Fabrication, characterization, and perceptions," *Sensors Journal, IEEE*, vol. 13, no. 10, pp. 4065–4080, 2013.

[21] A. N. Gent, *Engineering with rubber: how to design rubber components.* Carl Hanser Verlag GmbH Co KG, 2012.

[22] P. Atkins and J. de Paula, *Atkins' physical chemistry.* Oxford University Press, 2002.

[23] M. Ying, A. P. Bonifas, N. Lu, Y. Su, R. Li, H. Cheng, A. Ameen, Y. Huang, and J. A. Rogers, "Silicon nanomembranes for fingertip electronics," *Nanotechnology*, vol. 23, no. 34, p. 344004, 2012.

[24] H.-J. Kim, C. Son, and B. Ziaie, "A multiaxial stretchable interconnect using

liquid-alloy-filled elastomeric microchannels," *Applied Physics Letters*, vol. 92, no. 1, p. 011904, 2008.

[25] S. Nambiar and J. T. Yeow, "Conductive polymer-based sensors for biomedical applications," *Biosensors and Bioelectronics*, vol. 26, no. 5, pp. 1825–1832, 2011.

[26] C. Majidi, R. Kramer, and R. Wood, "A non-differential elastomer curvature sensor for softer-than-skin electronics," *Smart Materials and Structures*, vol. 20, no. 10, p. 105017, 2011.

[27] R. K. Kramer, C. Majidi, R. Sahai, and R. J. Wood, "Soft curvature sensors for joint angle proprioception," pp. 1919–1926, 2011.

[28] F. L. Hammond, R. K. Kramer, Q. Wan, R. D. Howe, and R. J. Wood, "Soft tactile sensor arrays for micromanipulation," in *Intelligent Robots and Systems (IROS), 2012 IEEE/RSJ International Conference on*. IEEE, 2012, pp. 25–32.

[29] F. L. Hammond III, R. K. Kramer, Q. Wan, R. D. Howe, and R. J. Wood, "Soft tactile sensor arrays for force feedback in micromanipulation," *IEEE Sensors Journal*, vol. 14, no. 5, p. 1443, 2014.

[30] Y.-L. Park, C. Majidi, R. Kramer, P. Bérard, and R. J. Wood, "Hyperelastic pressure sensing with a liquid-embedded elastomer," *Journal of Micromechanics and Microengineering*, vol. 20, no. 12, p. 125029, 2010.

[31] Y.-L. Park, B.-R. Chen, and R. J. Wood, "Design and fabrication of soft artificial skin using embedded microchannels and liquid conductors," *Sensors Journal, IEEE*, vol. 12, no. 8, pp. 2711–2718, 2012.

[32] Y.-L. Park, B.-r. Chen, and R. J. Wood, "Soft artificial skin with multimodal sensing capability using embedded liquid conductors," in *IEEE Sensors*. In-Teh, 2011, pp. 343–52.

[33] J. Ulmen and M. Cutkosky, "A robust, low-cost and low-noise artificial skin for human-friendly robots," in *Robotics and Automation (ICRA), 2010 IEEE International Conference on*. IEEE, 2010, pp. 4836–4841.

[34] P. Roberts, D. D. Damian, W. Shan, T. Lu, and C. Majidi, "Soft-matter capacitive sensor for measuring shear and pressure deformation," in *Robotics and Automation (ICRA), 2013 IEEE International Conference on*. IEEE, 2013, pp. 3529–3534.

[35] Y.-L. Park, D. Tepayotl-Ramirez, R. J. Wood, and C. Majidi, "Influence of cross-sectional geometry on the sensitivity and hysteresis of liquid-phase electronic pressure sensors," *Applied Physics Letters*, vol. 101, no. 19, 2012.

[36] F. P. Melchels, J. Feijen, and D. W. Grijpma, "A review on stereolithography and its applications in biomedical engineering," *Biomaterials*, vol. 31, no. 24, pp. 6121–6130, 2010.

[37] D. Dimitrov, K. Schreve, and N. De Beer, "Advances in three dimensional printing-state of the art and future perspectives," *Journal for New Generation Sciences*, vol. 4, no. 1, pp. p–21, 2006.

[38] D. B. Hall, P. Underhill, and J. M. Torkelson, "Spin coating of thin and ultrathin polymer films," *Polymer Engineering & Science*, vol. 38, no. 12, pp. 2039–2045, 1998.

[39] R. C. Chiechi, E. A. Weiss, M. D. Dickey, and G. M. Whitesides, "Eutectic gallium–indium (egain): A moldable liquid metal for electrical characterization of self-assembled monolayers," *Angewandte Chemie*, vol. 120, no. 1, pp. 148–150, 2008.

[40] J. F. Keithley, M. A. Hrusch-Tupta, and J. Yeager, *Low level measurements*. Keithley, 2000.

[41] H. Packard, "Hp 34401a multimeter users guide," *Hewlett Packard Company*.

[42] J. Fraden, *Handbook of modern sensors: physics, designs, and applications.* Springer, 2004.

[43] T. L. Anderson, *Fracture mechanics: fundamentals and applications.* CRC press, 2005.

[44] J.-B. Chossat, Y.-L. Park, R. J. Wood, and V. Duchaine, "A soft strain sensor based on ionic and metal liquids," *Sensors Journal, IEEE*, vol. 13, no. 9, pp. 3405–3414, 2013.

Appendices

Ecoflex-0030 Technical Bulletin

Ecoflex® Series

Super-Soft, Addition Cure Silicone Rubbers

www.smooth-on.com

PRODUCT OVERVIEW

Ecoflex® rubbers are platinum-catalyzed silicones that are versatile and easy to use. **Ecoflex®** rubbers are mixed 1A:1B by weight or volume and cured at room temperature with negligible shrinkage. Rubber also cures without a "tacky" surface. Low viscosity ensures easy mixing and de-airing, or you can choose to mix and dispense using our convenient dispensing cartridges.

Cured rubber is very soft, very strong and very "stretchy", stretching many times its original size without tearing and will rebound to its original form without distortion. **Ecoflex®** rubbers are water white translucent and can be color pigmented with Silc Pig® pigments for creating a variety of color effects. You can also add Smooth-On's Silicone Thinner® to further lower the viscosity. THI-VEX® silicone thickener can be added by weight to Ecoflex® 5 or Ecoflex® 00-10 for brushable aplications. ***Note: THI-VEX® is NOT compatible with Ecoflex® 00-30, Ecoflex® 00-20 or Ecoflex® 00-50.***

Soft, Softer, Softest . . . **Ecoflex®** rubbers are based on Smooth-On's Dragon Skin® technology and are currently available in four different hardness': Shore A-5, Shore 00-10, 00-20, 00-30 and 00-50. They are suitable for a variety of applications including making prosthetic appliances, cushioning for orthotics and special effects applications (especially in animatronics where repetitive motion is required). **Ecoflex® 5** has a pot life of 1 minute and a demold time of 5 minutes – Available only in dispensing cartridges.

TECHNICAL OVERVIEW

	Mixed Viscosity (ASTM D-2393)	Specific Gravity (g/cc) (ASTM D-1475)	Specific Volume (cu. in./lb.) (ASTM D-1475)	Pot Life (ASTM D-2471)	Cure Time	Shore Hardness (ASTM D-2240)	Tensile Strength (ASTM D-412)	100% Modulus (ASTM D-412)	Elongation at Break % (ASTM D-412)	Die B Tear Strength (ASTM D-624)	Shrinkage (in./in.) (ASTM D-2566)
Ecoflex® 5	13,000 cps	1.07	25.8	1 min.	5 min.	5A	350 psi	15 psi	1000%	75 pli	< .001 in./in.
Ecoflex® 00-50	8,000 cps	1.07	25.9	18 min.	3 hours	00-50	315 psi	12 psi	980%	50 pli	< .001 in./in.
Ecoflex® 00-30	3,000 cps	1.07	26.0	45 min.	4 hours	00-30	200 psi	10 psi	900%	38 pli	< .001 in./in.
Ecoflex® 00-20	3,000 cps	1.07	26.0	30 min.	4 hours	00-20	160 psi	8 psi	845%	30 pli	< .001 in./in.
Ecoflex® 00-10	14,000 cps	1.04	26.6	30 min.	4 hours	00-10	120 psi	8 psi	800%	22 pli	< .001 in./in.

*All values measured after 7 days at 73°F/23°C

Mix Ratio: 1A:1B by volume or weight
Color: Translucent
Useful Temperature Range: -65°F to 450°F (-53°C to 232°C)
Dielectric Strength (ASTM D-147-97a)***:*** >350 volts/mil

PROCESSING RECOMMENDATIONS

PREPARATION... Safety – Use in a properly ventilated area ("room size" ventilation). Wear safety glasses, long sleeves and rubber gloves to minimize contamination risk. Wear vinyl gloves only. Latex gloves will inhibit the cure of the rubber.

Store and use material at room temperature (73°F/23°C). Warmer temperatures will drastically reduce working time and cure time. Storing material at warmer temperatures will also reduce the usable shelf life of unused material. These products have a limited shelf life and should be used as soon as possible.

Cure Inhibition – Addition-cure silicone rubber may be inhibited by certain contaminants in or on the pattern to be molded resulting in tackiness at the pattern interface or a total lack of cure throughout the mold. Latex, tin-cure silicone, sulfur clays, certain wood surfaces, newly cast polyester, epoxy or urethane rubber may cause inhibition. If compatibility between the rubber and the surface is a concern, a small-scale test is recommended. Apply a small amount of rubber onto a non-critical area of the pattern. Inhibition has occurred if the rubber is gummy or uncured after the recommended cure time has passed.

Because no two applications are quite the same, a small test application to determine suitability for your project is recommended if performance of this material is in question.

To prevent inhibition, one or more coatings of a clear acrylic lacquer applied to the model surface is usually effective. Allow any sealer to thoroughly dry before applying rubber. Note: Even with a sealer, platinum silicones will not work with modeling clays containing heavy amounts of sulfur. Do a small scale test for compatibility before using on your project.

Safety First!

The Material Safety Data Sheet (MSDS) for this or any Smooth-On product should be read prior to use and is available upon request from Smooth-On. All Smooth-On products are safe to use if directions are read and followed carefully.

Keep Out of Reach of Children

Be careful. Use only with adequate ventilation. Contact with skin and eyes may cause irritation. Flush eyes with water for 15 minutes and seek immediate medical attention. Remove from skin with waterless hand cleaner followed by soap and water.

Important: The information contained in this bulletin is considered accurate. However, no warranty is expressed or implied regarding the accuracy of the data, the results to be obtained from the use thereof, or that any such use will not infringe upon a patent. User shall determine the suitability of the product for the intended application and assume all risk and liability whatsoever in connection therewith.

Applying A Release Agent - Although not usually necessary, a release agent will make demolding easier when pouring into or over most surfaces. Ease Release® 200 is a proven release agent for use with silicone rubber. Mann Ease Release® products are available from Smooth-On or your Smooth-On distributor.

IMPORTANT: To ensure thorough coverage, lightly brush the release agent with a soft brush over all surfaces of the model. Follow with a light mist coating and let the release agent dry for 30 minutes.

If there is any question about the effectiveness of a sealer/release agent combination, a small-scale test should be made on an identical surface for trial.

MEASURING & MIXING...

Before you begin, pre-mix Part B thoroughly. After dispensing required amounts of Parts A and B into mixing container (1A:1B by volume or weight), **mix thoroughly for 3 minutes making sure that you scrape the sides and bottom of the mixing container several times.** After mixing parts A and B, vacuum degassing is recommended to eliminate any entrapped air. Vacuum material for 2-3 minutes (29 inches of mercury), making sure that you leave enough room in container for product volume expansion.

POURING, CURING & MOLD PERFORMANCE...

For best results, pour your mixture in a single spot at the lowest point of the containment field. Let the rubber seek its level up and over the model. **A uniform flow will help minimize entrapped air.** The liquid rubber should level off at least 1/2" (1.3 cm) over the highest point of the model surface.

Curing / Post Curing - Allow rubber to cure as prescribed at room temperature (73°F/23°C) before demolding. Do not cure rubber where temperature is less than 65°F/18°C. **Optional:** Post curing the mold will aid in quickly attaining maximum physical and performance properties. After curing at room temperature, expose the rubber to 176°F/80°C for 2 hours and 212°F/100°C for one hour. Allow mold to cool to room temperature before using.

If Using As A Mold - When first cast, silicone rubber molds exhibit natural release characteristics. Depending on what is being cast into the mold, mold lubricity may be depleted over time and parts will begin to stick. No release agent is necessary when casting wax or gypsum. Applying a release agent such as Ease Release® 200 (available from Smooth-On) prior to casting polyurethane, polyester and epoxy resins is recommended to prevent mold degradation.

Thickening Ecoflex® Silicones - THI-VEX® may be added into Ecoflex® 5 & 00-10 by weight. The recommended maximum amount of THI-VEX® is 2% by weight. ***THI-VEX® thickener is not compatible with Ecoflex® 00-30, 00-20 or 00-50.*** An alternative for thickening Ecoflex® silicones is to add Ure-Fil® 9 or Ure-Fil® 11.

Thinning Ecoflex® Silicones - Smooth-On's Silicone Thinner® will lower the viscosity of Ecoflex® silicones for easier pouring and vacuum degassing. A **disadvantage** is that ultimate tear and tensile are reduced in proportion to the amount of Silicone Thinner® added. ***It is not recommended to exceed 10% by weight of total system (A+B).*** See the Silicone Thinner® technical bulletin (available from Smooth-On or your Smooth-On distributor) for full details.

Mold Performance & Storage - The physical life of the mold depends on how you use it (materials cast, frequency, etc.). Casting abrasive materials such as concrete can quickly erode mold detail, while casting non-abrasive materials (wax) will not affect mold detail. Before storing, the mold should be cleaned with a soap solution and wiped fully dry. Two part (or more) molds should be assembled. Molds should be stored on a level surface in a cool, dry environment.

SMOOTH-ON SINCE 1895

Call Us Anytime With Questions About Your Application.

Toll-free: **(800) 762-0744** Fax: **(610) 252-6200**

The new **www.smooth-on.com** is loaded with information about mold making, casting and more.

062612 - JR

Experimental Data

Table 1: Experimental results from the calibration procedure of the strain sensor with 800μm microchannels.

R (Ω)	**ΔR** (Ω)	**ΔR/R**	**ΔL** (mm)	**Lf** (mm)	**Strain**	**T ΔR** (Ω)
0,982	0	0	0	23	0	0
1,005	0,023	0,022886	0,5	23,5	0,021739	0,000375
1,028	0,046	0,044747	1	24	0,043478	0,000764
1,054	0,072	0,068311	1,5	24,5	0,065217	0,001168
1,072	0,09	0,083955	2	25	0,086957	0,001589
1,111	0,129	0,116112	2,5	25,5	0,108696	0,002027
1,149	0,167	0,145344	3	26	0,130435	0,002482
1,225	0,243	0,198367	3,5	26,5	0,152174	0,002956
2,75	1,768	0,642909	4	27	0,173913	0,00345
1,317	0,335	0,254366	4,5	27,5	0,195652	0,003964
1,396	0,414	0,296562	5	28	0,217391	0,0045
1,463	0,481	0,328776	5,5	28,5	0,23913	0,005059
1,554	0,572	0,368082	6	29	0,26087	0,005642
1,711	0,729	0,426067	6,5	29,5	0,282609	0,00625
2,068	1,086	0,525145	7	30	0,304348	0,006885
2,134	1,152	0,539831	7,5	30,5	0,326087	0,007549
2,354	1,372	0,582838	8	31	0,347826	0,008242
2,576	1,594	0,618789	8,5	31,5	0,369565	0,008966
2,914	1,932	0,663006	9	32	0,391304	0,009724
3,315	2,333	0,703771	10	33	0,434783	0,011348
3,578	2,596	0,725545	11	34	0,478261	0,013131
3,769	2,787	0,739453	12	35	0,521739	0,015092
3,906	2,924	0,748592	13	36	0,565217	0,017254
4,05	3,068	0,757531	14	37	0,608696	0,019645
4,383	3,401	0,775953	15	38	0,652174	0,022297
4,52	3,538	0,782743	16	39	0,695652	0,025245
4,6	3,618	0,786522	16,5	39,5	0,717391	0,026844
4,653	3,671	0,788953	17	40	0,73913	0,028533
4,923	3,941	0,800528	17,5	40,5	0,76087	0,030321
5,861	4,879	0,832452	18	41	0,782609	0,032214
5,962	4,98	0,83529	18,5	41,5	0,804348	0,034221
6,248	5,266	0,84283	19	42	0,826087	0,036349
6,651	5,669	0,852353	19,5	42,5	0,847826	0,038609
6,892	5,91	0,857516	20	43	0,869565	0,041012
7,458	6,476	0,868329	20,5	43,5	0,891304	0,043569
7,33	6,348	0,86603	21	44	0,913043	0,046293
7,86	6,878	0,875064	21,5	44,5	0,934783	0,049198
8,21	7,228	0,88039	22	45	0,956522	0,0523
8,639	7,657	0,886329	22,5	45,5	0,978261	0,055617
8,931	7,949	0,890046	23	46	1	0,059168

Table 2: Experimental results from the calibration procedure of the strain sensor with 800μm microchannels.

R(Ω)	**ΔR** (Ω)	**ΔR/R**	**ΔL** (mm)	**Lf** (mm)	**Strain**	**T ΔR** (Ω)
0,982	0	0,982	0	23	0	0
1,005	0,023	1,005	0,5	23,5	0,021739	0,000375
1,028	0,046	1,028	1	24	0,043478	0,000764
1,054	0,072	1,054	1,5	24,5	0,065217	0,001168
1,072	0,09	1,072	2	25	0,086957	0,001589
1,111	0,129	1,111	2,5	25,5	0,108696	0,002027
1,149	0,167	1,149	3	26	0,130435	0,002482
1,225	0,243	1,225	3,5	26,5	0,152174	0,002956
2,75	1,768	2,75	4	27	0,173913	0,00345
1,317	0,335	1,317	4,5	27,5	0,195652	0,003964
1,396	0,414	1,396	5	28	0,217391	0,0045
1,463	0,481	1,463	5,5	28,5	0,23913	0,005059
1,554	0,572	1,554	6	29	0,26087	0,005642
1,711	0,729	1,711	6,5	29,5	0,282609	0,00625
2,068	1,086	2,068	7	30	0,304348	0,006885
2,134	1,152	2,134	7,5	30,5	0,326087	0,007549
2,354	1,372	2,354	8	31	0,347826	0,008242
2,576	1,594	2,576	8,5	31,5	0,369565	0,008966
2,914	1,932	2,914	9	32	0,391304	0,009724
3,315	2,333	3,315	10	33	0,434783	0,011348
3,578	2,596	3,578	11	34	0,478261	0,013131
3,769	2,787	3,769	12	35	0,521739	0,015092
3,906	2,924	3,906	13	36	0,565217	0,017254
4,05	3,068	4,05	14	37	0,608696	0,019645
4,383	3,401	4,383	15	38	0,652174	0,022297
4,52	3,538	4,52	16	39	0,695652	0,025245
4,6	3,618	4,6	16,5	39,5	0,717391	0,026844
4,653	3,671	4,653	17	40	0,73913	0,028533
4,923	3,941	4,923	17,5	40,5	0,76087	0,030321
5,861	4,879	5,861	18	41	0,782609	0,032214
5,962	4,98	5,962	18,5	41,5	0,804348	0,034221
6,248	5,266	6,248	19	42	0,826087	0,036349
6,651	5,669	6,651	19,5	42,5	0,847826	0,038609
6,892	5,91	6,892	20	43	0,869565	0,041012
7,458	6,476	7,458	20,5	43,5	0,891304	0,043569
7,33	6,348	7,33	21	44	0,913043	0,046293
7,86	6,878	7,86	21,5	44,5	0,934783	0,049198
8,21	7,228	8,21	22	45	0,956522	0,0523
8,639	7,657	8,639	22,5	45,5	0,978261	0,055617
8,931	7,949	8,931	23	46	1	0,059168

Table 3: Experimental results from the calibration procedure of the sensor with 400μm microchannels.

R(Ω)	**ΔR** (Ω)	**ΔR/R**	**ΔL**(mm)	**Lf** (mm)	**Strain**	**T ΔR** (Ω)
4,389	0	0	0	23	0	0
4,604	0,215	0,046699	1	24	0,043478	0,001018
4,749	0,36	0,075805	2	25	0,086957	0,002119
4,831	0,442	0,091492	3	26	0,130435	0,00331
4,91	0,521	0,10611	4	27	0,173913	0,0046
5,224	0,835	0,159839	5	28	0,217391	0,006
5,234	0,845	0,161444	5,5	28,5	0,23913	0,006746
5,313	0,924	0,173913	6	29	0,26087	0,007523
5,309	0,92	0,173291	6,5	29,5	0,282609	0,008334
5,363	0,974	0,181615	7	30	0,304348	0,00918
5,404	1,015	0,187824	7,5	30,5	0,326087	0,010065
5,443	1,054	0,193643	8	31	0,347826	0,010989
5,485	1,096	0,199818	8,5	31,5	0,369565	0,011955
5,544	1,155	0,208333	9	32	0,391304	0,012966
5,439	1,05	0,19305	9,5	32,5	0,413043	0,014024
5,819	1,43	0,245747	10	33	0,434783	0,015131
5,825	1,436	0,246524	10,5	33,5	0,456522	0,016291
5,866	1,477	0,25179	11	34	0,478261	0,017508
5,877	1,488	0,25319	11,5	34,5	0,5	0,018783
5,969	1,58	0,264701	12	35	0,521739	0,020122
6,082	1,693	0,278362	12,5	35,5	0,543478	0,021528
6,18	1,791	0,289806	13	36	0,565217	0,023006
6,229	1,84	0,295393	13,5	36,5	0,586957	0,024559
6,289	1,9	0,302115	14	37	0,608696	0,026194
6,3487	1,9597	0,308677	14,5	37,5	0,630435	0,027915
6,396	2,007	0,31379	15	38	0,652174	0,029729
6,462	2,073	0,320799	15,5	38,5	0,673913	0,031641
6,512	2,123	0,326014	16	39	0,695652	0,03366
6,57	2,181	0,331963	16,5	39,5	0,717391	0,035791
6,689	2,3	0,343848	17	40	0,73913	0,038045
6,872	2,483	0,361321	17,5	40,5	0,76087	0,040428
5,526	1,137	0,205755	18	41	0,782609	0,042953
5,564	1,175	0,211179	18,5	41,5	0,804348	0,045628
5,59	1,201	0,214848	19	42	0,826087	0,048466
5,635	1,246	0,221118	19,5	42,5	0,847826	0,051479
5,662	1,273	0,224832	20	43	0,869565	0,054683
5,714	1,325	0,231887	20,5	43,5	0,891304	0,058092
5,756	1,367	0,237491	21,5	44,5	0,934783	0,065597
4,956	0,567	0,114407	22	45	0,956522	0,069733
4,969	0,58	0,116724	23	46	1	0,07889

Table 4: Experimental results from the calibration procedure of the strain sensor with 600μm microchannels.

R(Ω)	**ΔR** (Ω)	**ΔR/R**	**ΔL** (mm)	**Lf** (mm)	**Strain**	**T ΔR** (Ω)
0,782	0	0	0	23	0	0
0,783	0,001	0,0013	1,5	24,5	0,065217	0,001557966
0,785	0,003	0,0038	2	25	0,086957	0,002118946
0,794	0,012	0,0153	2,5	25,5	0,108696	0,002702477
0,802	0,02	0,0256	3	26	0,130435	0,003309686
0,935	0,153	0,1957	3,5	26,5	0,152174	0,00394177
0,984	0,202	0,2583	4	27	0,173913	0,0046
1,231	0,449	0,5742	4,5	27,5	0,195652	0,005285727
1,498	0,716	0,9156	5	28	0,217391	0,006000387
1,562	0,78	0,9974	5,5	28,5	0,23913	0,00674551
1,624	0,842	1,0767	6	29	0,26087	0,007522725
1,717	0,935	1,1957	6,5	29,5	0,282609	0,008333769
1,833	1,051	1,344	7	30	0,304348	0,009180493
2,017	1,235	1,5793	7,5	30,5	0,326087	0,010064876
2,122	1,34	1,7136	8	31	0,347826	0,01098903
2,215	1,433	1,8325	8,5	31,5	0,369565	0,011955216
2,361	1,579	2,0192	9	32	0,391304	0,012965851
2,505	1,723	2,2033	9,5	32,5	0,413043	0,014023526
2,746	1,964	2,5115	10	33	0,434783	0,015131019
2,837	2,055	2,6279	10,5	33,5	0,456522	0,016291309
3,154	2,372	3,0332	11	34	0,478261	0,0175076
3,346	2,564	3,2788	11,5	34,5	0,5	0,018783333
3,614	2,832	3,6215	12	35	0,521739	0,020122215
3,984	3,202	4,0946	12,5	35,5	0,543478	0,021528236
4,343	3,561	4,5537	13	36	0,565217	0,023005702
4,621	3,839	4,9092	13,5	36,5	0,586957	0,024559264
4,896	4,114	5,2609	14	37	0,608696	0,026193945
5,365	4,583	5,8606	14,5	37,5	0,630435	0,027915185
5,96	5,178	6,6215	15	38	0,652174	0,029728876
6,821	6,039	7,7225	15,5	38,5	0,673913	0,031641411
7,23	6,448	8,2455	16	39	0,695652	0,033659733
7,608	6,826	8,7289	16,5	39,5	0,717391	0,035791396
7,923	7,141	9,1317	17	40	0,73913	0,038044625
8,92	8,138	10,407	17,5	40,5	0,76087	0,040428393
9,549	8,767	11,211	18	41	0,782609	0,0429525
9,89	9,108	11,647	18,5	41,5	0,804348	0,045627666
10,58	9,798	12,529	19	42	0,826087	0,048465638
11,298	10,516	13,448	19,5	42,5	0,847826	0,051479306
11,65	10,868	13,898	20	43	0,869565	0,05468284
11,968	11,186	14,304	20,5	43,5	0,891304	0,058091845
12,357	11,575	14,802	21	44	0,913043	0,061723536
12,953	12,171	15,564	21,5	44,5	0,934783	0,065596939
13,584	12,802	16,371	22	45	0,956522	0,069733125
13,965	13,183	16,858	22,5	45,5	0,978261	0,074155478
14,289	13,507	17,272	23	46	1	0,07889

Table 5: Experimental results from the calibration procedure of the pressure sensor with 800μm microchannels (Trial 1).

Force(N)	**Pressure** (Pa)	**R** (Ω)	**ΔR**(Ω)	**T ΔR** (Ω)
0	0	0,6036	0	0
0,2	500	0,638	0,0344	1,47709E-08
0,4	1000	0,6031	-0,0005	2,9685E-08
0,6	1500	0,6029	-0,0007	4,47443E-08
0,8	2000	0,6027	-0,0009	5,99511E-08
1	2500	0,6028	-0,0008	7,53074E-08
1,2	3000	0,6025	-0,0011	9,08155E-08
1,4	3500	0,6026	-0,001	1,06478E-07
1,6	4000	0,6028	-0,0008	1,22296E-07
1,8	4500	0,6025	-0,0011	1,38273E-07
2	5000	0,6023	-0,0013	1,54412E-07
2,2	5500	0,6028	-0,0008	1,70714E-07
2,4	6000	0,6032	-0,0004	1,87182E-07
2,6	6500	0,6032	-0,0004	2,03818E-07
2,8	7000	0,6032	-0,0004	2,20626E-07
3	7500	0,6038	0,0002	2,37608E-07
3,2	8000	0,6038	0,0002	2,54766E-07
3,4	8500	0,6032	-0,0004	2,72104E-07
3,6	9000	0,6031	-0,0005	2,89623E-07
3,8	9500	0,6036	0	3,07328E-07
4	10000	0,604	0,0004	3,25221E-07
4,2	10500	0,6038	0,0002	3,43305E-07
4,4	11000	0,6037	1E-04	3,61583E-07
4,6	11500	0,604	0,0004	3,80058E-07
4,8	12000	0,6038	0,0002	3,98734E-07
5	12500	0,6031	-0,0005	4,17614E-07
5,4	13500	0,6038	0,0002	4,55997E-07
5,8	14500	0,6042	0,0006	4,95237E-07
6,2	15500	0,6043	0,0007	5,35362E-07
6,6	16500	0,6043	0,0007	5,76402E-07
7	17500	0,6048	0,0012	6,18389E-07
7,4	18500	0,6048	0,0012	6,61357E-07
7,8	19500	0,6042	0,0006	7,0534E-07
8,2	20500	0,6047	0,0011	7,50374E-07
8,6	21500	0,6052	0,0016	7,96497E-07
9	22500	0,6052	0,0016	8,4375E-07
9,4	23500	0,605	0,0014	8,92175E-07
9,8	24500	0,6055	0,0019	9,41815E-07
10,2	25500	0,6058	0,0022	9,92717E-07
10,6	26500	0,6059	0,0023	1,04493E-06
11	27500	0,6059	0,0023	1,09851E-06
11,5	28750	0,6061	0,0025	1,16747E-06

Table 6: Experimental results from the calibration procedure of the pressure sensor with 800μm microchannels (Trial 1).

Force(N)	**Pressure** (Pa)	**R** (Ω)	**ΔR**(Ω)	**T ΔR** (Ω)
12	30000	0,6064	0,0028	1,23876E-06
12,5	31250	0,6066	0,003	1,3125E-06
13	32500	0,6071	0,0035	1,38881E-06
13,5	33750	0,6075	0,0039	1,46783E-06
14	35000	0,6078	0,0042	1,5497E-06
14,5	36250	0,6077	0,0041	1,63459E-06
15	37500	0,6077	0,0041	1,72266E-06
15,5	38750	0,608	0,0044	1,81409E-06
16	40000	0,6097	0,0061	1,90909E-06
16,5	41250	0,61	0,0064	2,00786E-06
17	42500	0,6101	0,0065	2,11064E-06
17,5	43750	0,6101	0,0065	2,21767E-06
18	45000	0,6104	0,0068	2,32923E-06
18,5	46250	0,6105	0,0069	2,44559E-06
19	47500	0,6108	0,0072	2,5671E-06
19,5	48750	0,611	0,0074	2,69408E-06
20	50000	0,6117	0,0081	2,82692E-06
20,5	51250	0,6135	0,0099	2,96604E-06
21	52500	0,6138	0,0102	3,1119E-06
22	55000	0,614	0,0104	3,42585E-06
23	57500	0,6177	0,0141	3,77344E-06
24	60000	0,6183	0,0147	4,16038E-06
25	62500	0,6192	0,0156	4,59375E-06
26	65000	0,6205	0,0169	5,08245E-06
27	67500	0,6225	0,0189	5,63778E-06
28	70000	0,6244	0,0208	6,27439E-06
29	72500	0,627	0,0234	7,01151E-06
30	75000	0,6289	0,0253	0,000007875
31	77500	0,6314	0,0278	8,90039E-06
32	80000	0,634	0,0304	1,01379E-05
33	82500	0,639	0,0354	1,16611E-05
34	85000	0,6451	0,0415	1,35815E-05
35	87500	0,6509	0,0473	1,60781E-05
36	90000	0,6617	0,0581	1,94559E-05
37	92500	0,6693	0,0657	2,42813E-05
38	95000	0,6845	0,0809	3,17386E-05
39	97500	0,6987	0,0951	4,47891E-05
40	100000	0,7291	0,1255	7,35E-05
41	102500	0,7557	0,1521	0,000188344
43	107500	0,8615	0,2579	-9,8766E-05
45	112500	1,184	0,5804	-4,1344E-05
47	117500	1,5036	0,9	-2,6988E-05
49	122500	2,1446	1,541	-2,0463E-05
51	127500	3,018	2,4144	-1,6734E-05
53	132500	4,0524	3,4488	-1,4322E-05
55	137500	5,36	4,7564	-1,2633E-05

Table 7: Experimental results from the calibration procedure of the pressure sensor with 800μm microchannels (Trial 2).

Force(N)	**Pressure** (Pa)	**R** (Ω)	**ΔR**(Ω)	**T ΔR** (Ω)
0	0	0,6223	0	0
1	2500	0,6223	0	-1,7E-06
2	5000	0,6224	1E-04	-1,6E-06
3	7500	0,6224	1E-04	-1,6E-06
4	10000	0,6225	0,0002	-1,6E-06
5	12500	0,6224	1E-04	-1,6E-06
6	15000	0,6225	0,0002	-1,6E-06
7	17500	0,6225	0,0002	-1,6E-06
8	20000	0,6227	0,0004	-1,6E-06
9	22500	0,623	0,0007	-1,6E-06
10	25000	0,6231	0,0008	-1,6E-06
11	27500	0,6232	0,0009	-1,6E-06
12	30000	0,6231	0,0008	-1,6E-06
13	32500	0,6233	0,001	-1,6E-06
14	35000	0,6234	0,0011	-1,6E-06
15	37500	0,6235	0,0012	-1,6E-06
16	40000	0,6234	0,0011	-1,6E-06
17	42500	0,6246	0,0023	-1,6E-06
18	45000	0,6249	0,0026	-1,6E-06
19	47500	0,6371	0,0148	-1,6E-06
20	50000	0,6329	0,0106	-1,6E-06
21	52500	0,6327	0,0104	-1,6E-06
22	55000	0,6323	0,01	-1,6E-06
23	57500	0,6335	0,0112	-1,6E-06
24	60000	0,6329	0,0106	-1,6E-06
25	62500	0,6326	0,0103	-1,6E-06
26	65000	0,6338	0,0115	-1,6E-06
27	67500	0,634	0,0117	-1,6E-06
28	70000	0,6359	0,0136	-1,6E-06
29	72500	0,6374	0,0151	-1,6E-06
30	75000	0,6383	0,016	-1,6E-06
31	77500	0,6404	0,0181	-1,6E-06
32	80000	0,6441	0,0218	-1,6E-06
33	82500	0,6456	0,0233	-1,6E-06
34	85000	0,6484	0,0261	-1,6E-06
35	87500	0,6689	0,0466	-1,6E-06
36	90000	0,6754	0,0531	-1,6E-06
37	92500	0,6923	0,07	-1,6E-06
38	95000	0,6994	0,0771	-1,6E-06
39	97500	0,7009	0,0786	-1,6E-06
40	100000	0,7015	0,0792	-1,6E-06
41	102500	0,725	0,1027	-1,6E-06

Table 8: Experimental results from the calibration procedure of the pressure sensor with 800μm microchannels (Trial 2).

Force(N)	**Pressure** (Pa)	**R** (Ω)	Δ**R**(Ω)	**T** Δ**R** (Ω)
42	105000	0,713	0,0907	-1,6E-06
43	107500	0,7358	0,1135	-1,6E-06
44	110000	0,7614	0,1391	-1,6E-06
45	112500	0,82	0,1977	-1,6E-06
46	115000	0,984	0,3617	-1,6E-06
47	117500	1,15	0,5277	-1,6E-06
48	120000	1,495	0,8727	-1,6E-06
49	122500	1,813	1,1907	-1,6E-06
50	125000	2,28	1,6577	-1,6E-06
51	127500	2,86	2,2377	-1,6E-06
52	130000	3,648	3,0257	-1,6E-06
53	132500	4,056	3,4337	-1,6E-06
54	135000	5,2241	4,6018	-1,6E-06
55	137500	5,8425	5,2202	-1,6E-06
56	140000	6,3178	5,6955	-1,6E-06
57	142500	7,0256	6,4033	-1,6E-06
58	145000	9,894	9,2717	-1,6E-06

Table 9: Experimental results from the calibration procedure of the pressure sensor with 800μm microchannels (Trial 3).

Force(N)	**Pressure** (Pa)	**R** (Ω)	**ΔR**(Ω)	**T ΔR** (Ω)
0	0	1,071	0	0
1	2500	1,071	0	7,7E-08
2	5000	1,072	0,001	1,62E-07
3	7500	1,071	0	2,55E-07
4	10000	1,072	0,001	3,59E-07
5	12500	1,073	0,002	4,74E-07
6	15000	1,073	0,002	6,04E-07
7	17500	1,074	0,003	7,51E-07
8	20000	1,071	0	9,19E-07
9	22500	1,074	0,003	1,11E-06
10	25000	1,074	0,003	1,34E-06
11	27500	1,074	0,003	1,6E-06
12	30000	1,075	0,004	1,92E-06
13	32500	1,075	0,004	2,3E-06
14	35000	1,076	0,005	2,78E-06
15	37500	1,076	0,005	3,39E-06
16	40000	1,076	0,005	4,2E-06
17	42500	1,076	0,005	5,32E-06
18	45000	1,077	0,006	6,96E-06
19	47500	1,077	0,006	9,63E-06
20	50000	1,075	0,004	1,47E-05
21	52500	1,076	0,005	2,81E-05
22	55000	1,077	0,006	0,000162
23	57500	1,077	0,006	-4,8E-05
24	60000	1,078	0,007	-2,2E-05
25	62500	1,078	0,007	-1,5E-05
27	67500	1,078	0,007	-9,2E-06
29	72500	1,078	0,007	-7E-06
31	77500	1,079	0,008	-5,8E-06
33	82500	1,079	0,008	-5E-06
35	87500	1,105	0,034	-4,5E-06
37	92500	1,425	0,354	-4,1E-06
37,5	93750	1,503	0,432	-4E-06
38	95000	1,478	0,407	-3,9E-06
38,5	96250	1,501	0,43	-3,9E-06
39	97500	1,586	0,515	-3,8E-06
39,5	98750	1,708	0,637	-3,7E-06
40	100000	1,773	0,702	-3,7E-06

Table 10: Experimental results from the calibration procedure of the pressure sensor with 800μm microchannels (Trial 3).

Force(N)	**Pressure** (Pa)	**R** (Ω)	**ΔR**(Ω)	**T ΔR** (Ω)
40,5	101250	1,828	0,757	-3,6E-06
41	102500	1,916	0,845	-3,6E-06
41,5	103750	1,987	0,916	-3,5E-06
42	105000	2,116	1,045	-3,5E-06
42,5	106250	2,372	1,301	-3,4E-06
43	107500	2,418	1,347	-3,4E-06
43,5	108750	2,487	1,416	-3,3E-06
44	110000	2,971	1,9	-3,3E-06
44,5	111250	3,058	1,987	-3,3E-06
45	112500	3,303	2,232	-3,2E-06
45,5	113750	4,226	3,155	-3,2E-06
46	115000	4,608	3,537	-3,2E-06
46,5	116250	4,957	3,886	-3,1E-06
47	117500	5,912	4,841	-3,1E-06
47,5	118750	6,039	4,968	-3,1E-06
48	120000	6,314	5,243	-3E-06
48,5	121250	6,69	5,619	-3E-06
49	122500	6,936	5,865	-3E-06
49,5	123750	7,418	6,347	-3E-06
50	125000	7,77	6,699	-2,9E-06
50,5	126250	8,678	7,607	-2,9E-06
51	127500	8,984	7,913	-2,9E-06
51,5	128750	9,249	8,178	-2,9E-06
52	130000	9,59	8,519	-2,9E-06